INTRACAVITY LASER ABSORPTION SPECTROSCOPY USING QUANTUM CASCADE LASER AND FABRY-PEROT INTERFEROMETER

by

GAUTAM MEDHI
M.Sc. Indian Institute of Technology Guwahati, 2005

A dissertation submitted in partial fulfillment of the requirements
for the degree of Doctor of Philosophy
in the Department of Physics
in the College of Sciences
at the University of Central Florida
Orlando, Florida

Fall Term
2011

Major Professor: Robert E. Peale

ABSTRACT

Intracavity Laser Absorption Spectroscopy (ICLAS) at IR wavelengths offers an opportunity for spectral sensing of low vapor pressure compounds. We report here an ICLAS system design based on a quantum cascade laser (QCL) at THz (69.9 μm) and IR wavelengths (9.38 and 8.1 μm) with an open external cavity. The sensitivity of such a system is potentially very high due to extraordinarily long effective optical paths that can be achieved in an active cavity. Sensitivity estimation by numerical solution of the laser rate equations for the THz QCL ICLAS system is determined. Experimental development of the external cavity QCL is demonstrated for the two IR wavelengths, as supported by appearance of fine mode structure in the laser spectrum. The 8.1 μm wavelength exhibits a dramatic change in the output spectrum caused by the weak intracavity absorption of acetone. Numerical solution of the laser rate equations yields a sensitivity estimation of acetone partial pressure of 165 mTorr corresponding to ~ 200 ppm. The system is also found sensitive to the humidity in the laboratory air with an absorption coefficient of just 3×10^{-7} cm^{-1} indicating a sensitivity of 111 ppm. Reported also is the design of a compact integrated data acquisition and control system. Potential applications include military and commercial sensing for threat compounds such as explosives, chemical gases, biological aerosols, drugs, banned or invasive organisms, bio-medical breath analysis, and terrestrial or planetary atmospheric science.

.

Dedicated to my Parents

ACKNOWLEDGMENTS

I would like to thank my advisor Dr. Robert E. Peale for allowing me to work in his research group. This research would not have been its present shape without his constant supports, streaming knowledge and ideas. I would also like to thank him for supporting me financially for these many years.

I would like to thank Dr. Leonid Chernyak, Dr. Masahiro Ishigami and Dr. Peter Delfyett for serving on my dissertation committee and spending their time reading it and evaluating it.

I would like to thank, Dr. Andrey Muravjov for his supports, guidance and contribution to this work. He stood behind me all the time, listening to me patiently and advising me. I would like to thank Mr. Chris Fredricksen for his help in Labview. Moreover, numerous suggestions and helps, I got from him, will never be forgotten.

I would like to thank, Dr. Himanshu Saxena for design and machine shop works and Dr. Justin Cleary for his input in the simulation part.

I would take the opportunity to say thanks to David Bradford for his help in the machine shop. Thanks go to Ray Ramotar also for numerous helps.

This research was funded by Zyberwear, Inc, (Oliver Edwards, President) via Army Phase I and II SBIR (Dr. Dwight Woolard, Program Manager) without which this work would not have been initiated and completed. I am very thankful for their support. I would also like to thank the Department of Physics for their support.

I would like to acknowledge my colleagues Dr. Tatiana Brusentsova, Janardan Nath, Nima Nader-Esfahani, Deep Panjwani, Monas Shahzad, Farnood Khalilzadeh-Rezaie, Pedro Figueiredo, Doug Moukonen and Jonathon Arnold for their support.

I would also like to thank my friends Pankaj Kadwani, Balasubramaniam Lingam, and Prabhu Doss Mani for being nice to me for these many years.

Above all I would like to thank my parents and brother for their constant love, support and encouragement, which has made all this work possible.

TABLE OF CONTENTS

LIST OF FIGURES

CHAPTER 1: INTRODUCTION

1.1 Background

Light Amplification by Stimulated Emission of Radiation (LASER) is one of the most useful tools for spectroscopy due to its unique properties. The primary attention, for a long time, was to make the laser spectral emission linewidth narrower and thus, make its peak power very high. Thus broadband multimode laser received less attention. However, in cases of broad gain spectrum, lasers have unique application in spectroscopy, viz., high sensitivity of the output emission spectral distribution to frequency dependent cavity losses [1]. This property of laser along with good collimation, high spectral power density and wide tunability has paved the way for the development of many fundamentally new methods of spectral analysis.

Among the various spectral analysis techniques, absorption spectroscopy is one of the widely used and highly sensitive techniques. The general method for measuring absorption spectra of molecules or atoms is based on the determination of the absorption coefficient from the spectral intensity transmitted through a sample. The absorption coefficient of permissible transitions of molecules or atoms depends linearly on their concentrations through their absorption cross-section. The minimum still-detectable concentrations of absorbing molecules are determined by the noise power, the absorption cross-section of the transition or the transition strength, the incident radiation power and the absorption path length. The principle sources of noise are detector noise, intensity fluctuations of incident radiation (technical noise) and the

random fluctuations of the absorbing molecules [2]. The technical noise, which represents the major limitation, decreases with increasing frequency and thus, can be reduced by various frequency and wavelength modulation techniques. Sensitivity enhancement and detection of small variations in the optical density of the absorber can also be obtained by these techniques [2]. A larger linestrength is obtained when the transitions occur in the fundamental vibrational band of the molecules. Thus, working in the mid-IR region, where molecules have fundamental vibrational bands, the system detection sensitivity can be increased effectively.

1.2 Motivation

Sensitivity of an absorption spectroscopy technique also depends on the effective optical path length through the Beer-Lambert law given by, $T(\nu) = e^{-\alpha(\upsilon)d}$ where *T(ν)* and *α(ν)* are the frequency dependent transmittance and absorption coefficient and *d* is the optical path length. Thus, the third way to enhance the sensitivity is to make the effective optical path length longer. A longer path length is usually accomplished in a 'White cell' [3] through multiple reflections between two high reflecting mirrors as shown in Fig. 1.1. The number of required reflections for small absorption coefficient (low vapor pressure) absorbers is huge to get a reasonably detectable signal in a 'White cell'.

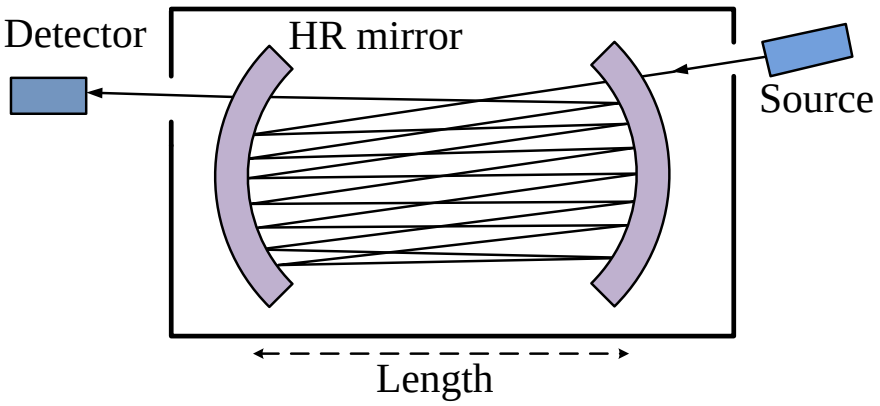

Figure 1.1 : Schematic of a 'White cell' with multiple reflections.

Fig 1.2 shows the saturated vapor pressures and absorption coefficients of a few explosives [4] along with acetone for comparison. The absorption coefficients are calculated considering an optimistic molecular absorption cross-section of 10^{-18} cm^2 [5]. Note the vapor pressures and absorption coefficients are very small for explosives, in comparison to a volatile substance such as acetone. Fig. 1.3 shows the optical path length needed for 1% transmission change due to saturated vapor of the same explosives.

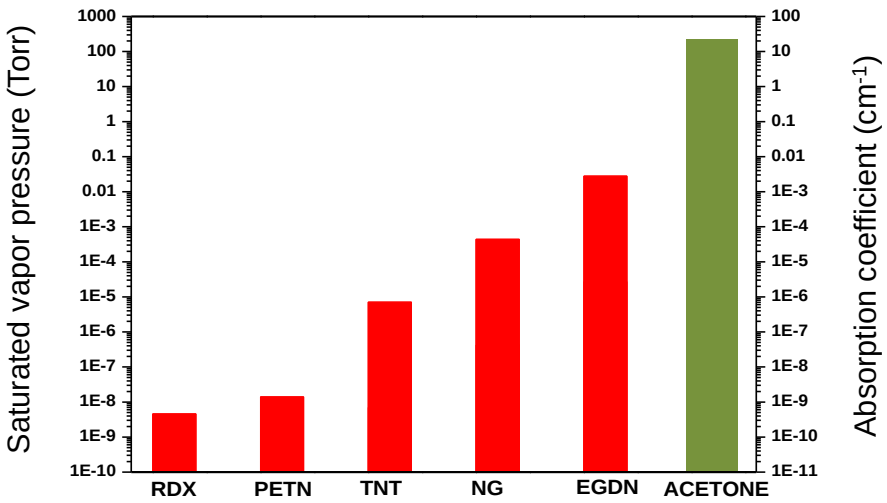

Figure 1.2 : Saturated vapor pressures and absorption coefficients of a few common explosives compared with acetone.

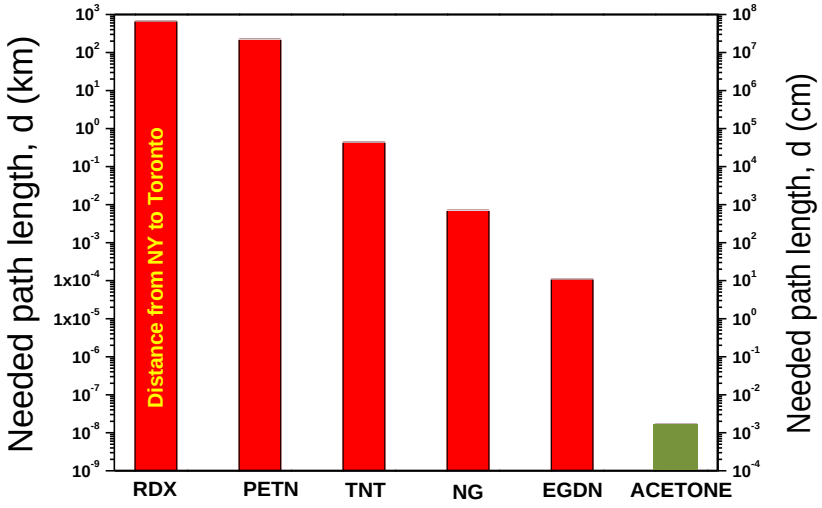

Figure 1.3 : Needed path length of few explosives to get 1% transmission change in a White cell. The path length is compared with acetone.

For a conventional laboratory 'White cell' of half a meter length, the number of reflections needed to get 1 km long path sufficient for a detectable 1% change in transmission is around

1000 for TNT. Each reflection incurs loss due to the finite reflectivity of metal mirrors. Fig 1.4 plots the intensity remaining in a passive cavity as a function of the number of reflections. Arrows indicate the number of reflections needed to obtain 1% transmittance change for various explosives. The transmitted signal, on the other hand, drops to zero after only ~ 100 reflections even when the mirrors have a reflectivity of 99% (Fig 1.4). A conventional 'White cell' is, thus, insufficient to measure absorption of low vapor pressure compounds. This challenge is overcome using Intracavity Laser Absorption Spectroscopy (ICLAS), where broadband gain medium is placed inside the cavity, such that it compensates losses from the optical elements, and thereby produces a very long effective path length. Thus the detection sensitivity is enhanced considerably in ICLAS, in favorable cases by several orders of magnitude.

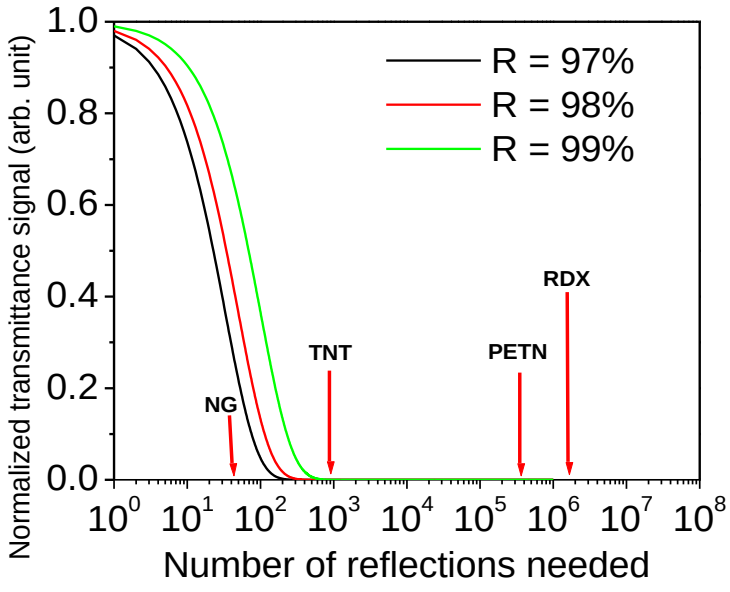

Figure 1.4 : Number of reflections needed in a 'White cell' to get 1% transmission change.

1.3 Intracavity Laser Absorption Spectroscopy (ICLAS)

Multimode, broadband ICLAS was first suggested in 1970 [6]. It consists of quenching the laser emission spectrum at a particular frequency of interest of the absorber placed inside the cavity. The laser oscillates on many resonator modes simultaneously, is amplified due to many resonator round trips, and finally concentrates to a spectral region with highest gain. The absorber's frequencies are not amplified during this process, but rather it imprints its signature on the laser emission spectrum. The time evolution of the laser emission spectrum shows a dip in its intensity at the absorber's frequency, which can be recorded by ordinary spectroscopic instrumentation. In ICLAS the laser itself is a nonlinear detector of weak absorption and therefore the parameters of an intracavity spectrometer are determined by the mechanism of lasing process [6]. It is usually advantageous for the broadband gain of the laser to exceed the absorber linewidth.

The high sensitivity in an ICLAS system is achieved by four different effects [2].

(i) For a resonators with two mirrors of reflectivity $R_1 = 1$ and $R_2 = 1\text{-}T_2$, (neglecting mirror absorption, where T_2 is the mirror transmissivity), if the absorbed power is measured directly through the resulting pressure increase on the absorption cell or through the laser induced fluorescence, the signal will be $1/T_2$ times larger than for the case of single pass absorption outside the cavity. The sensitivity enhancement in detecting small absorptions does not have any direct correlation with the gain medium and can also be realized in external passive resonators also. The radiation power inside the passive cavity will be enhanced by the same factor

if the laser output is mode matched by optical elements into the fundamental mode of the passive cavity.

(ii) The dependence of a single-mode laser output power on intracavity absorption losses also affects the sensitivity of detection. The enhancement factor of the sensitivity for a homogeneously broadened gain is given by $\frac{g_o}{\gamma(\gamma-g_o)}$, where g_o is the gain at no pump power and γ is the intracavity loss. At pump power far above the threshold, the unsaturated gain is large compared to the losses and the sensitivity enhancement factor depends inversely on the losses. If these losses are due to mirror transmission, then this enhancement will be ~ $1/T_2$. But just above the threshold, unsaturated gain is almost equal to the losses, and in this case a tremendous enhancement can be obtained, though limited by increasing instability of the laser output and spontaneous radiation.

The above two effects are true when the laser oscillates in a single mode. Larger enhancement can be achieved when the lasers oscillates simultaneously in several competing modes.

(iii) In a broad homogenous spectral gain profile, all the molecules contribute simultaneously to the gain of all modes with frequencies within the homogeneous linewidth. Thus different oscillating laser modes share the same molecules to achieve their gains. This leads to mode competition and mode coupling (considering mode coupling and mode frequencies are time independent). Strong mode coupling can suppress a mode completely if it is tuned into the resonance with an intracavity absorption line.

(iv) Any external perturbation prevents stationary conditions in multimode lasers and thus, the coupling and the frequencies of the modes depend on time. Thus a specific mode can exist in a multimode laser for a finite amount of average time, called the mode lifetime (t_m). If the measuring time of the intracavity absorption exceeds the mode lifetime, then no information about the absorption coefficients can be obtained. Thus the laser is pumped by a step function pump profile starting at $t = 0$ and remains constant. The intracavity absorption is measured in the time interval $0 < t < t_m$. The time evolution of the laser intensity in a specific mode with a specific frequency after the start of the pump pulse depends on the gain profile of the laser medium, the absorption coefficient of the intracavity sample and the mean mode lifetime. The spectral width of the laser output becomes narrower with time, but the absorption dips become more pronounced.

Since the method has been suggested in 1970, different gain media have been used for this technique. An early broadband laser applied to ICLAS was the flash lamp-pumped Nd^{3+}-doped glass laser [7][8][9]. An effective optical path length of 300 km had been obtained with this laser for 1 ms pulse duration [7][8] with a maximum path length of 3600 km for 12 ms [9]. Weak absorption spectra of CO_2, CH_4, C_2H_2, C_2HD, NH_3 [10] and H_2O, HN_3, HCN [11] have been recorded in the 1.055 to 1.067 μm spectral range. The sensitivity of the system with this laser is limited by the laser pulse duration. The most widely used laser with ICLAS is multimode dye laser. The spectral ranges covered by these lasers are in visible and near IR. The maximum path length obtained by these lasers is 70,000 km operated at pulse duration of 230 ms [12]. The sensitivity is limited by the nonlinear interaction of light and gain medium, namely by

four wave mixing (FWM) due to population inversion [13]. Ti:sapphire laser is good for sensitive ICLAS application. It covers a spectral range from 0.67 to 1.1 μm. The sensitivity of this laser in ICLAS ranges from 50 km [14] to 1300 km [15]. The dominant limitations for this type of laser are coming from FWM and Rayleigh scattering (RS). Color center lasers (CCL), for ICLAS operation, comparatively cover a wide spectral range from 0.6 to 3 μm [16]. Though CCL extend into the mid-IR region where fundamental vibrations of many molecules occur, it usually requires liquid nitrogen cooling to operate and its spectrum condenses to a very narrow width due to small spectral gain [17]. Convenient CCLs include LiF:F_2^+ [18][19] and LiF:F_2^- [20][21] that operate at room temperature with broad gain. The effective path length obtained with CCL is 120 km operated at 400 μs pulse duration [22]. The sensitivity of ICLAS with this laser is limited by the laser pulse duration. GaAlAs diode lasers are also used extensively for ICLAS at 770 nm [23] and 780 nm [24][25]. The obtained effective path length is comparatively small (40 km at 130 μs pulse duration [25]) and is limited by spontaneous emission (SE). Mostly limited by RS, Nd^{3+} doped fiber laser gives an effective optical path length of 130 km at 430 μs.

Unfortunately, all these lasers operate somewhere from the ultraviolet to the near infrared region and the whole MID-IR region has been unexplored by this technique due to lack of a suitable gain medium. Meanwhile, most trace gases, explosives and biological aerosols have their unique absorption features in this molecular fingerprint region (λ = 3-12 μm), and thus, this range is of great importance to defense and homeland security, environmental monitoring, medical diagnostic, etc. Moreover large absorption cross-sections (e.g. 10^{-18} cm^2 for acetone [5])

in this region provide high detection sensitivity. In the near-IR region, only overtone and combination bands are accessible, where molecular absorption line strengths are several orders of magnitude smaller than those in the mid-IR region. Common mid-IR coherent sources are lead-salt diode lasers and sources based on optical parametric oscillators (OPO) in nonlinear crystals. Bad thermal conductivity and poor mechanical stability makes lead-salt lasers less attractive for ICLAS applications [8]. Nonlinear crystals require cascaded two-step pumping arrangements, resulting in lower conversion efficiency governed by Manley-Rowe limit [8]. The threshold power becomes very high and CW operation remains challenging [8] for these crystals.

All these difficulties are overcome with the revolutionary invention of quantum cascade laser (QCL), which operate over the whole mid-IR range.

1.4 Quantum cascade laser (QCL)

In a conventional semiconductor laser, the so-called 'active region' consists of sandwich between two different semiconductor materials arranged in a double heterostructure, forming a p-n junction. The electron or hole is injected into the active region where they recombine and create a photon. Specially designed cladding layers around the active region constrain the generated photons, which are forced to bounce between two specially coated facets that act as the traditional mirrors of a laser cavity. As the radiation is created by the recombination process of the electron in the conduction band and the holes in the valence band, the wavelength of the emitted photon depends on the minimum energy difference between the two bands, called the

band gap, which determines the optical properties of the materials. Thus different semiconductor materials are needed to obtain different wavelength lasers.

Quantum cascade laser (QCL), on the other hand, is based on one type of charge carrier, the electrons, and is therefore a unipolar laser [26]. The lasing process depends on an entirely different mechanism, called intersubband transitions [27], where electrons from higher energy states jump to lower energy states in a quantum well within the same conduction band. Thus, QCL contains a series of quantum wells or electron traps, which are ultrathin sandwiches of two different semiconductor materials. The thicknesses of these wells are typically a few nanometers and the electrons are confined primarily to the center part of these sandwiches. The motion of the electrons in the perpendicular direction of the layers is quantized, which gives rise to a series of discrete energy states. The difference in energy between two states can be controlled by changing the well thickness. Thus the wavelength can be tailored over a wide range, from mid-IR to far-IR, by using the same material but varying the well thickness.

The classical concept of a QCL is a repetitive periodic structure of active regions and injector regions in which a miniband is formed. From the injector miniband the electrons are injected into the upper laser energy level of the active section. Here the laser transition takes place, population inversion is created and maintained. After that, the lower laser energy level of the active region is emptied by LO-phonon emissions and the electrons enter the next injector region by tunneling. Here electron gets cooled down and ready to inject to the next active region. This process repeats typically for 10-100 period.

The performance of these devices has been increased tremendously, since the first QCL was demonstrated in 1994 [26]. Although QCL lasing has been achieved in the THz regime from 59 μm (5 THz) down to 350 μm (950 GHz) [28] with device fabricated in the GaAs material system and with pulsed operation up to 178 K [29][30], the best performances have been observed in the mid-IR region (3-12 μm) using a InGaAs/AlInAs/InP material system [8].

The first CW operation of QCL was reported in 2002 up to a temperature of 312 K, at an emission wavelength of 9.1 μm [31] and much of the mid-infrared region is now covered by CW operating QCL. Today multi watt output power in CW at room temperature with wall plug efficiency of 12.5% is also reported [32]. Fig 1.5 presents a plot of operating temperature of QCL both in pulsed and CW mode as a function of wavelength [33][34][35][36].

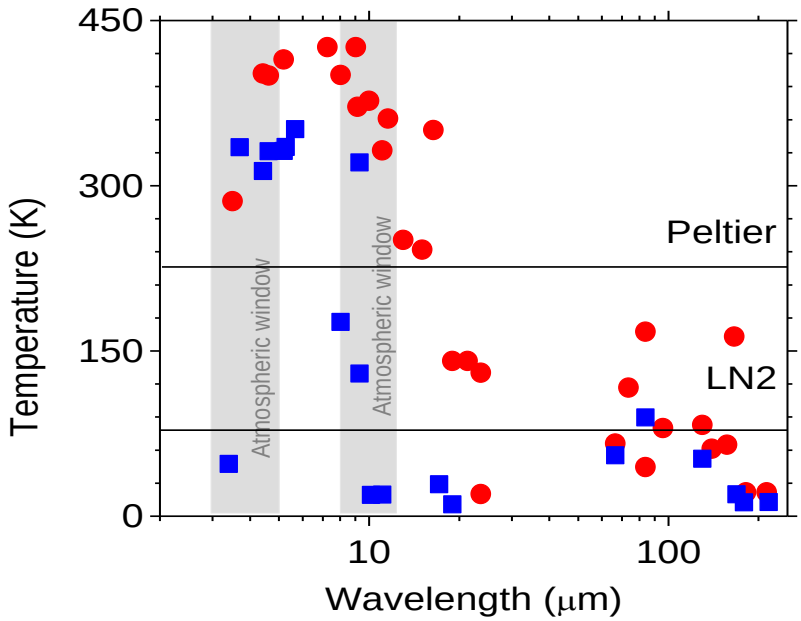

Figure 1.5 : Maximum operating temperature of QCL in pulsed mode (dots) and continuous wave (squares). The liquid N_2 (LN2) and Peltier temperatures are marked by the horizontal lines.

QCLs are especially appropriate for broadband applications for two reasons: (i) intersubband transitions are transparent on either side of their transition energy and (ii) cascading principle almost comes naturally because of the unipolar nature of the laser. These two features enable the cascading of dissimilar active region designs, emitting at different wavelengths to create a broadband emitter [37], which attracted a lot of attention for spectroscopic applications.

1.4.1 Distributed feedback (DFB) QCL

The characteristics the QCL needed to become useful for ordinary spectroscopy are (i) single frequency emission and (ii) the frequency tuning [8]. The simple QCL based on Fabry-Perot resonator can only be tuned in a very small range by varying the device temperature. The Fabry-Perot type QCL is good for producing high powers [38], but it typically is multi-mode, and unsuitable for usual spectroscopic application. However such lasers are ideal for the intracavity spectroscopy presented here.

Distributed feedback (DFB) QCL, on the other hand uses the same Fabry-Perot technique, except for a distributed Bragg reflector build on top of the waveguide to prevent emitting wavelength other than the desired one. The tuning is easy as it always works on single mode even at higher current. The first DFB QCL was demonstrated by Jerome Faist [39] and Claire Gmachl [40]. A room temperature DFB QCL was reported soon after that [41] and a high-resolution spectroscopy technique was demonstrated [42]. After that many groups have demonstrated a number of spectroscopic techniques for sensing purpose using DFB QCL [43].

As individual DFB QCL has a narrow tuning range, people are using DFB QCL array [44] and a wavelength span of 220 cm^{-1} was obtained using 32 DFB QCLs [45].

The limited tuning range of a DFB QCL can be overcome in a grating coupled external cavity QCL (EC-QCL) operation, which was first demonstrated in 2001 at cryogenic temperatures [46]. Soon after that, EC-QCL operation at 10.4 μm wavelength in pulsed mode at room temperature was reported in 2002 [47]. The maximum tuning range obtained in such a configuration was 54 cm^{-1} at 84 K and at 5.1 μm [48].

The invention of bound-to-continuum design [49] has provided a tremendously broad gain region with high gain and it accelerated the progress in the performance of EC-QCLs. The radiative transitions in such a design occur between a single initial state located close to the injection barrier and a quasiminiband of final states delocalized over the coupled quantum wells of a chirped superlattice [8]. A tuning range of 150 cm^{-1} was reported using this design in EC-QCL configuration at room temperature in pulsed mode at 10 μm wavelength [50].

This dissertation work presents an ICLAS system based on an external-cavity QCL in different resonator configurations. Contrary to the conventional grating based external cavity system either in Littrow [51] or Littman-Metcalf [52] configurations, this technique uses a Fabry-Perot interferometer outside the cavity as a real time spectral analyzer. A compact integrated control and data acquisition electronics (cRIO) architecture from National Instrument have been used as a development platform.

The subsequent chapters of this dissertation are organized in the following manner:

CHAPTER 2: This chapter gives the basic theoretical equations for an ICLAS system with Fabry-Perot interferometer. Equations governing the detection limit, laser dynamics, sensitivity estimation of an ICLAS system and free spectral range (FSR), finesse, and resolving power of Fabry-Perot interferometer are discussed here.

CHAPTER 3: This chapter discusses the numerical solution results of a THz QCL ICLAS system. The preliminary sensitivity estimation from laser rate equations is discussed here. The preliminary testing of a THz QCL and the required optics for Fabry-Perot interferometer are also mentioned here.

CHAPTER 4: External cavity operation of a mid-IR QCL at 9.38 μm is discussed in this chapter. The system design schematic, external cavity mode structure for this QCL and the resolution of the Fabry-Perot analyzer are presented.

CHAPTER 5: This chapter covers the demonstration of the external cavity configuration at 8.1 μm QCL wavelength. The sensitivity of the system in presence of acetone and different thickness polyethylene sheets inside the cavity are demonstrated here.

CHAPTER 6: The sensitivity of the 8.1 μm QCL ICLAS system in the presence of acetone vapor is discussed in this chapter. The estimated sensitivity by numerical solution based on the experimental results is presented.

CHAPTER 7: This chapter discusses the sensitivity of the 8.1 μm QCL ICLAS system when the laser spectrum is analyzed by Fabry-Perot interferometer. The system sensitivity in presence of water vapor in atmosphere and acetone vapor is discussed here.

CHAPTER 8: This chapter discusses the electronics system and software.

CHAPTER 9: Investigation of Fano reflectors as potential high reflectivity optics for Fabry-Perot analyzer is presented in this chapter.

CHAPTER 10: This chapter presents the infrared vapor spectrum of 2,4,6-trinitortoluene (TNT) measured by FTIR at different temperatures.

CHAPTER 11: The work that has been completed in this dissertation is summarized and future prospective is proposed in this chapter.

CHAPTER 2: THEORETICAL BACKGROUND

2.1 Principle of ICLAS

The schematic of a multimode QCL ICLAS is shown in Fig 2.1, where a homogeneously broadband gain media *G(v)* is inserted between two mirrors M_1 and M_2, forming the cavity. A sample of narrow absorbance linewidth *α(v)* is inserted in the cavity. For best application of multimode ICLAS, the homogeneously broadened gain of the laser should exceed the narrow linewidth of the sample. The laser light passes through the sample several times until intracavity absorption will be accumulated in the spectrum as in a multipass cell. In such a system the broadband cavity loss is compensated by the laser gain. The emission spectrum is extremely sensitive to the narrow linewidth absorption in the cavity because of the enormously long effective path length. The laser emission spectra can be recorded by a spectrometer or by other spectroscopic instrumentation [53].

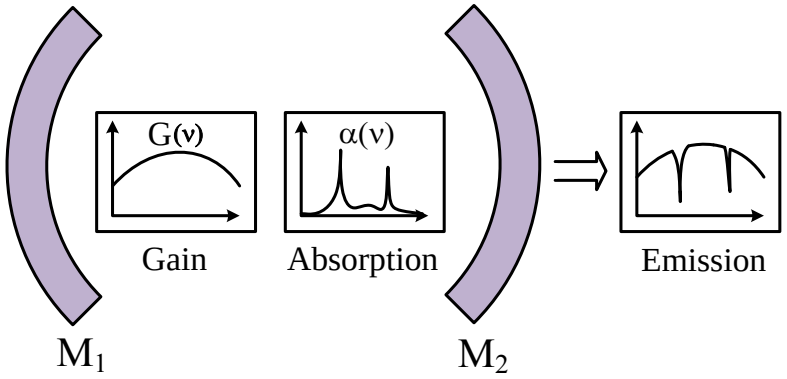

Figure 2.1 : Schematic of an ICLAS system. M_1 and M_2 are two mirrors. The gain medium stays inside the cavity to compensate the broadband optical losses, but the narrow intracavity absorption lines are seen as a dip in the laser emission spectrum.

2.2 Sensitivity estimation

The transmitted light passing through an absorber is governed by the Lambert-Beer law given by

$$I(\nu) = I_o(\nu)e^{-\alpha(\nu)d} \quad (2\text{-}1)$$

where $I(\nu)$ is the transmitted light, $I_0(\nu)$ is the incident light, $\alpha(\nu)$ and d are the frequency dependent absorption coefficient and optical path length of the absorber, respectively. The absorption coefficient is given by the absorber concentration n and frequency dependent absorption cross-section σ as

$$\alpha(\nu) = n\sigma(\nu) \quad (2\text{-}2)$$

The absorption signal or absorbance K in the transmitted spectrum is defined as

$$K(\nu) = \alpha(\nu)d = ln\frac{I_o}{I} \quad (2\text{-}3)$$

Minimum concentration required for the detection of the absorber is the key parameter that determines the scope of possible practical applications of an ICLAS technique. Spectral resolution and temporal resolution are also very crucial parameters determining the sensitivity of the system. The detection limit on the other hand is the most important parameter of such a system, defined as the smallest absorption coefficient α_{min} detectable in the transmitted spectrum. It is characterized by (i) signal-to-noise ratio (as discussed in section 1.1) and (ii) spectral

sensitivity, defined as the absorption signal per corresponding absorption coefficient. The spectral sensitivity, in general, can be written as an effective absorption path length,

$$d_{eff} = \frac{K(\nu)}{\alpha(\nu)} \quad (2\text{-}4)$$

Thus the detection limit is,

$$\alpha_{min} = \frac{K_{min}(\nu)}{\left(d_{eff}\right)_{max}} \quad (2\text{-}5)$$

where $K_{min}(\nu)$ is the noise equivalent absorption signal, and $(d_{eff})_{max}$ is the maximum value of the effective path length [47].

2.3 Spectral dynamics of a multimode laser

The temporal evolution of the emission spectra of a multimode laser and its response to the intracavity absorption is described by the rate equation, given by [53],

$$\frac{dM_q}{dt} = -\gamma M_q + B_q N\left(M_q + 1\right) - \alpha_q c M_q \quad (2\text{-}6)$$

$$\frac{dN}{dt} = P - AN - N\sum_q B_q M_q \quad (2\text{-}7)$$

Here γ is the broadband cavity loss (both due to mirror and waveguide), α_q is the absorption coefficient of intracavity absorption at the q-th axial laser mode, c is the velocity of light, P is the pump rate, and A is the rate of decay (both radiative and nonradiative) of the upper laser level. Laser inversion equals the population N of the upper laser level. These equations characterize the regimes of QCL laser build-up, namely the laser inversion N, the total photon number M, the photon number M_q in individual laser mode, and the final stability of the laser spectral output. The homogeneously broadened gain B_q of induced emission per photon in mode q can be approximated by a Lorentzian profile expressed by

$$B_q = \frac{B_o}{1 + \left(\frac{q - q_o}{Q}\right)^2} \qquad (2\text{-}8)$$

Here q is the mode number given by $q = \frac{2L}{\lambda_q}$, λ_q is the center wavelength of the q-th mode, B_o is the maximum gain at the central mode q_o and Q is the spectral width (half width half maximum, HWHM) of the laser gain.

After the pump power is switched on at $t = 0$, the laser dynamics extends over four time regions (i) the laser inversion N, (ii) the total photon number in the modes $M = \sum M_q$, (iii) the photon number M_q in individual laser mode and (iv) stationary spectral output. The first time region $t < t_{th}$ is characterized by the growth of the laser inversion, where inversion is smaller than that in the laser threshold and $M = 0$. The second region $t_{th} < t < t_M$ is characterized by stationary level, where the total photon number in the cavity starts growing exponentially until the inversion is depleted to its final stationary value $N = N_{th}$ at $t = t_M$ and the total photon number

reaches its stationary value. During $t > t_M$, laser inversion and the total photon number in the cavity stays stationary but the photon number in the individual laser mode still continues to vary [53]. The spectral dynamics of the laser output can be obtained by solving Eqs. 2.6 and 2.7 numerically.

2.4 Fabry-Perot interferometer

Fabry-Perot interferometer allows high-resolution spectroscopy. It uses multiple-beam interference and consists of two slightly wedged transparent plates with flat surfaces. The inner semitransparent, highly reflecting surfaces of the plates are set parallel to each other, while the outer surfaces are worked to make a small angle with each other, to eliminate multiple reflections from these surfaces. The transmitted intensity from the Fabry-Perot interferometer when the two flats are separated by a distance *l* is expressed as an Airy function,

$$I_T(\lambda) = \frac{(1-R)^2}{1+R^2-2Rcos\varphi} \qquad (2\text{-}9)$$

where *R* is the reflectivity of the two surfaces and

$$\varphi = \left(\frac{4\pi}{\lambda}\right) nlcos\theta \qquad (2\text{-}10)$$

Here θ is the incident angle within the interferometer and *n* is the refractive index of the medium between the two plates.

The free spectral range (FSR), define as the difference in the frequencies corresponding to successive peaks in the transmitted intensity for normal incidence is given by

$$FSR = \frac{c}{2nl} \tag{2-11}$$

This is a very important parameter as it corresponds to the range of frequencies that can be handled without successive orders overlapping. FSR is also related to the full width half maxima (FWHM) $\delta\nu$, of one of the transmission resonance as

$$F = \frac{FSR}{\delta\nu} = \frac{\pi\sqrt{R}}{1-R} \tag{2-12}$$

Here F is called the finesse, which defines the resolving power $Q = \frac{\lambda}{\Delta\lambda} = kF$ of the interferometer, and $k = l\frac{\lambda}{2}$ is the resonance order. From above equation, as the reflectivity approaches unity, the finesse becomes very high. For high reflectivity, the transmission maxima are narrow, so that the transmission of maxima of slightly different wavelengths can be easily distinguished. Because of this capability, the Fabry-Perot interferometer can be used as a high-resolution spectrometer.

CHAPTER 3: TERAHERTZ QCL ICLAS

3.1 Introduction

Terahertz (THz) frequency region (0.3 – 10 THz), which bridges the optical and radio-frequency domains [28], is historically characterized by a relative lack of convenient radiation source, detectors and transmission technology. It has remained one of the least developed spectral regions, although lots of work in the last decade has advanced its potential applications in many fields, viz., sensing, atmospheric and environmental sciences, biological sciences, threat detection, non-destructive evaluation, communications technology, ultrafast spectroscopy etc. [29], a particular interest is to detect and identify explosives by their THz absorption features. This chapter presents the numerical sensitivity estimation of a THz QCL ICLAS system working at 69.9 μm.

3.2 Sensitivity estimation

The sensitivity limit for a THz QCL-based ICLAS had been estimated by numerical solution of the laser rate Eqs 2.6 and 2.7. The numerical solution of Eqs. 2.6 and 2.7 can be presented as a time-integrated laser emission spectrum, as shown in Fig. 3.1, where a weak intracavity absorption line (Lorentzian shape) had been included. Fig. 3.1 displays the laser emission frequency corresponding to the THz QCL at 69.9 μm. The logarithmic abscissa represents the integration time, which can be interpreted as the laser-pulse duration. The signal

strength is indicated by a logarithmic color scale with blue being few photons and red being many. The red vertical stripe at 2 μs corresponds to a 600 m effective path. Fig. 3.2 presents both the intracavity absorber line profile, having the very low peak value of just 2 x 10^{-4} cm^{-1} and the laser emission profile. In a conventional transmittance experiment using a 10 cm vapor cell, the absorption dip in the intensity would have been only 0.2%, which would be lost in the noise. In contrast, the THz QCL ICLAS simulation reveals a nearly 100% deep absorption feature, which has been achieved due to the extraordinarily long intracavity path length.

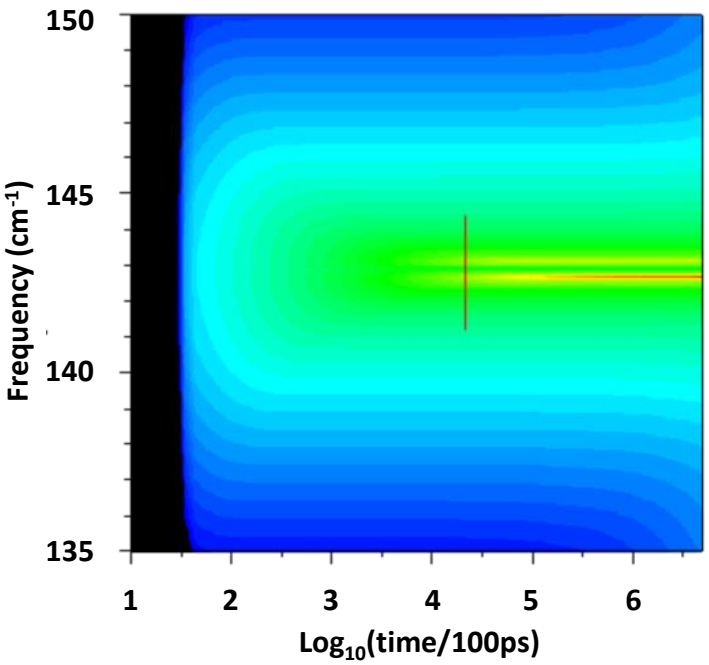

Figure 3.1 : Time integrated laser emission spectrum of a 69.9 μm THz QCL in presence of an intracavity absorber. The vertical line at 2 μs corresponds to an effective path length of 600 m.

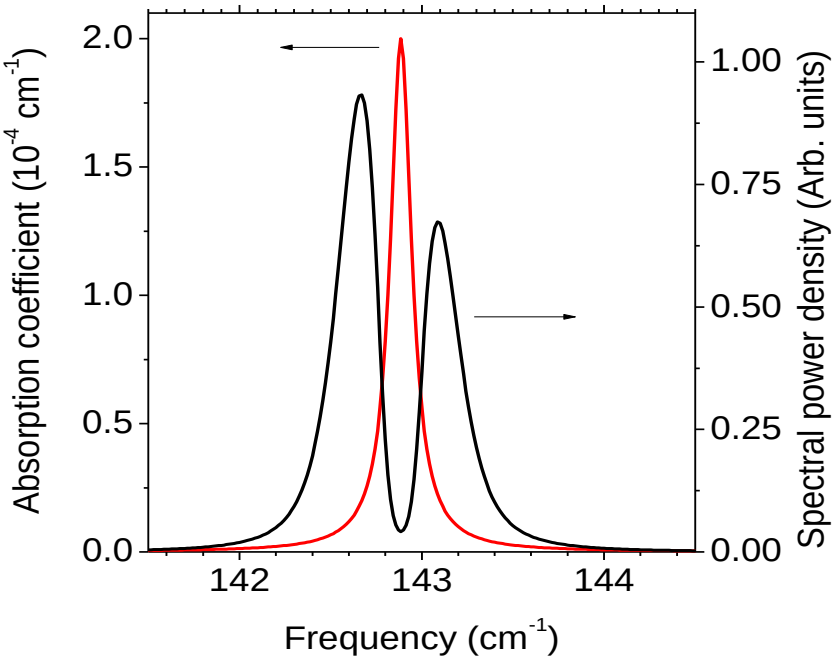

Figure 3.2 : Weak intracavity absorption profile (red) and its effect on the laser emission spectrum (black) at 2 μs integration time.

Similar simulations for typical THz QCL parameters with 2 μs pulse duration suggest that absorptions as weak as 10^{-6} cm^{-1} might be detected. Strong infrared molecular absorption cross sections are of the order of 10^{-18} cm^2 [5], which indicate a detection limit of 10^{12} molecules per cubic centimeter. In comparison with the number density of usual atmospheric molecules at standard conditions, this corresponds to 40 ppb. The saturated vapor pressure of TNT is 10^{-3} Pa [4], or 13 ppb, or 3 x 10^{11} molecules per cubic centimeter. In other words, the predicted sensitivity for a relatively short THz QCL pulse is within a factor of 3 needed to detect TNT in a confined space such as a shipping container. The needed increase can be achieved by increasing the pulse duration, which might easily be achieved by operating the laser closer to threshold, or by operating at a temperature slightly below 77 K, as might be achieved using a Stirling cooler.

A Fabry-Perot (FP) spectrum analyzer concept is shown conceptually in Fig. 3.3. The 69.9 μm QCL is housed in a liquid nitrogen cryostat, and its emission is collimated with an off-axis parabolic mirror and ideally sent out through the cryostat window to a 95% reflecting external cavity mirror. Target vapors pass through the open portion of the cavity. The 5% of the beam transmitted through the cavity mirror then passes a scanning central-spot FP interferometer and is collected by a detector. Calculated FP transmission as a function of FP gap for the laser spectrum of Fig. 3.1 is presented in Fig. 3.4, assuming an achievable THz FP finesse of 100. A near perfect representation of the laser spectrum of Fig. 3.1 is demonstrated in Fig. 3.4.

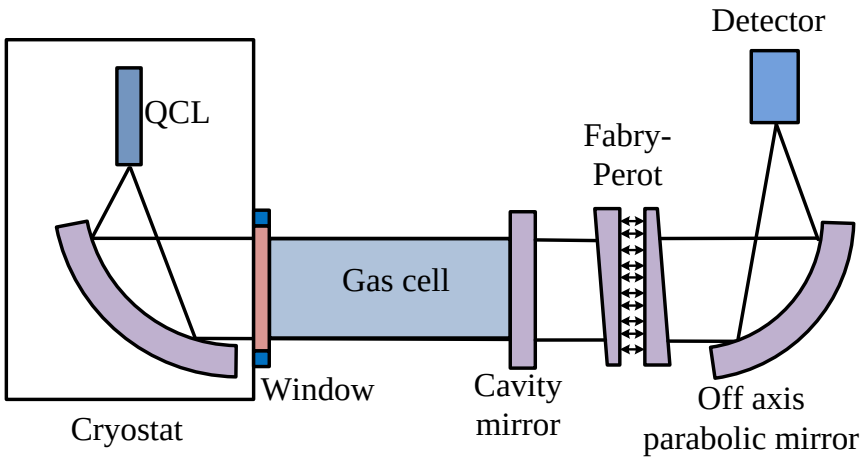

Figure 3.3 : A schematic of the 69.9 μm QCL ICLAS configuration with FP spectrum analyzer.

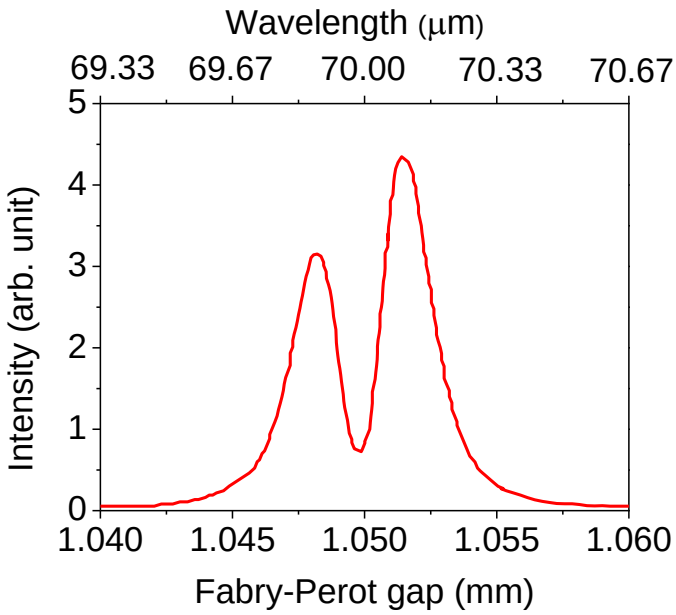

Figure 3.4 : 69.9 μm QCL spectrum measured by Fabry-Perot analyzer.

To collect the spectrum of Fig. 3.4, where 30 μm of mirror travel is required in 300 nm steps, 100 laser shots are required. Each laser shot requires about 60 μJ of electrical power, giving a requirement for the power supply of 6 mJ per spectrum. For comparison, a single 9 V battery stores 16,000 J of energy. Thus, battery operation is feasible, especially in the LWIR where the QCL requires no cryocooler.

3.3 Experimental details

Fig. 3.5 presents a photograph of the cryostat-mounted optics that were designed and fabricated for the THz QCL purchased from TRION. The laser was cooled to 77 K and excited by a laser diode driver with 10 μs x 1.4 A pulses at 20 Hz rep rate. The DEI laser diode driver

was externally triggered by a Stanford DG535 pulse generator operating in burst mode. Fifty pulses at 1 kHz rep rate, followed by 50 ms of no triggers achieves the 50% slow chopping needed for the Golay cell. The laser pulse duration was varied from 1 to 10 μs, giving an excitation duty cycle from 0.1 to 1 %. The collimated laser beam was collected outside the 25-μm-thick Mylar cryostat window by an off-axis parabolic mirror and focused onto the entrance aperture of a Golay cell. The Golay output was synchronously lock-in amplified. Measurements of lasing threshold are presented in Fig. 3.6. The trace for 10 μs pulse duration (1 % duty cycle) falls below the 5 μs trace because the laser overheats. The threshold current is about 0.95 A independent of pulse duration. At high current, the power tends to fall for the long pulses, again due to overheating.

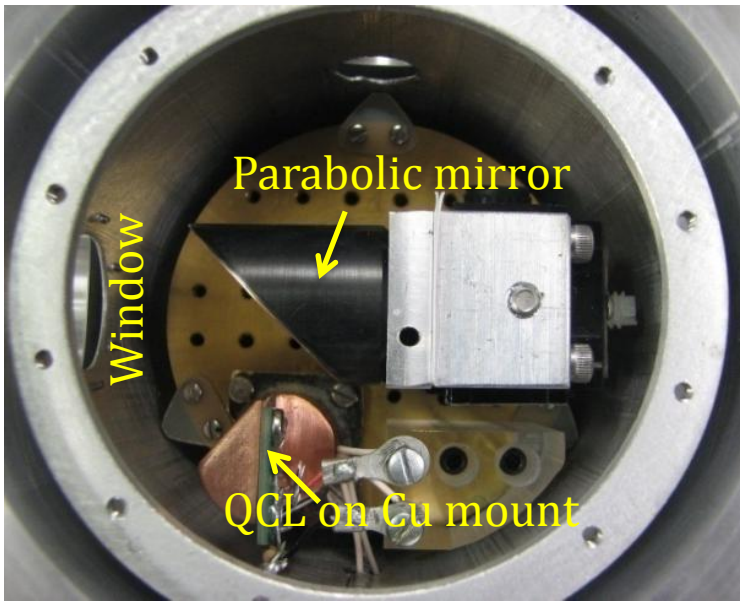

Figure 3.5: Mount and collimator for cryogenic external cavity for THz QCL.

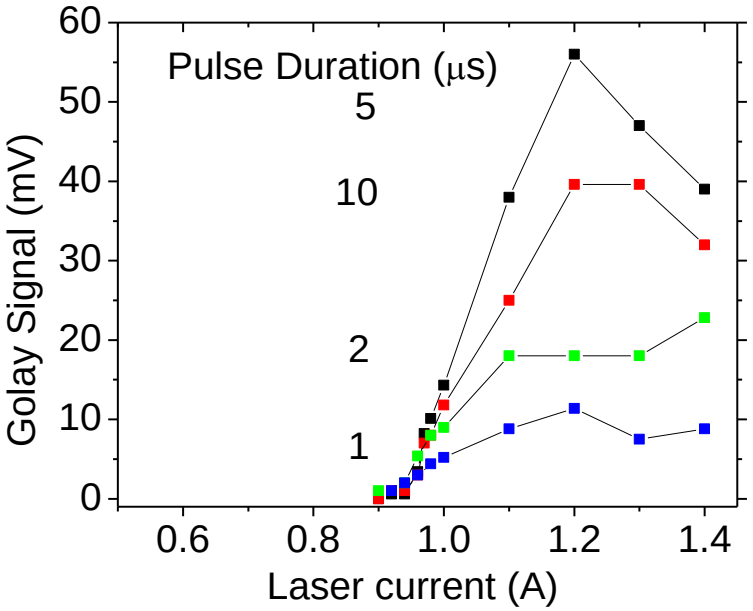

Figure 3.6 : Laser emission signal measured by a golay cell as a function of laser current for 4 different pulse durations. The laser overheats for 10 μs pulse durations, so the signal at 10 μs falls below 5 μs.

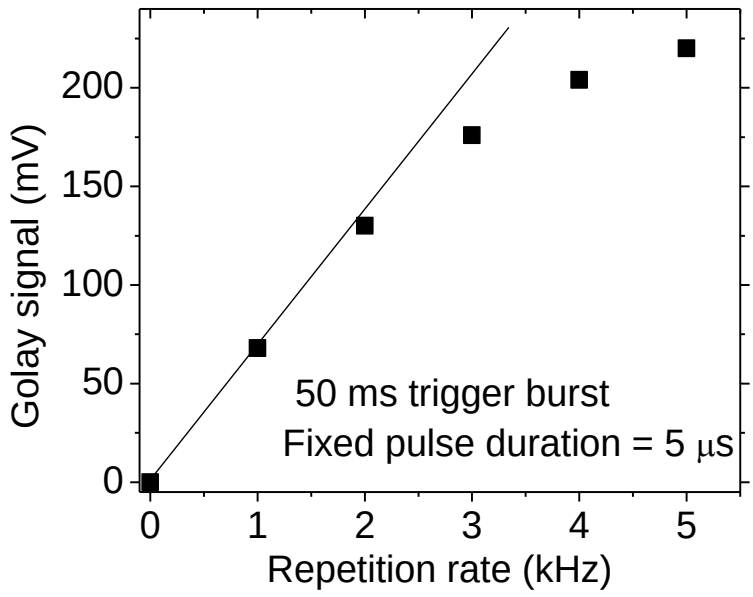

Figure 3.7 : Golay signal from the TRION THz QCL vs repetition rate, keeping the trigger burst parameters constant (50 ms of triggers followed by 50 ms of none) for constant 5 μs pulse durations.

Fig. 3.7 more clearly demonstrates the overheating effect. The duty cycles were increased through the values 0.5, 1.0, 1.5, 2.0, and 2.5%. The signal roll-off near 3 kHz indicates overheating, making clear the specified 3% duty limit. From the maximum achieved Golay signal, the Golay responsivity, the duty cycle, and pulse duration we obtain for the QCL an average power of 6.7 μW, peak power of 0.27 mW, and pulse energy of 1.3 nJ. Accounting for atmospheric absorption, we multiply these figures by 2 or more to get actual emission power at the laser end facet. This result is in reasonable agreement with TRION specifications.

Fig. 3.8 presents the measured beam profiles of the QCL in the horizontal and vertical direction near the cryostat window and at a distance of 2.5 cm from the window and the effect of atmospheric attenuation. The beam has a double peak in the horizontal scan both near the window and at 2.5 cm from the cryostat window and falls off more smoothly from the center in the vertical scan. The width of the profile is a bit less than the diameter of the output window and is probably defined primarily by the cold shield aperture diameter. Moving the detector back from the cryostat by 2.5 cm mainly decreases the intensity by the factor 0.63 with little beam divergence observed. From this is determined the absorption coefficient of the laboratory air at the specified 69.9 μm laser wavelength as 0.19 cm^{-1} or 0.81 dB/cm. Half of the power is lost in a distance of 3.7 cm. Nevertheless, even with no collection optic, the Golay can still detect laser signal at a distance of 0.5 meter.

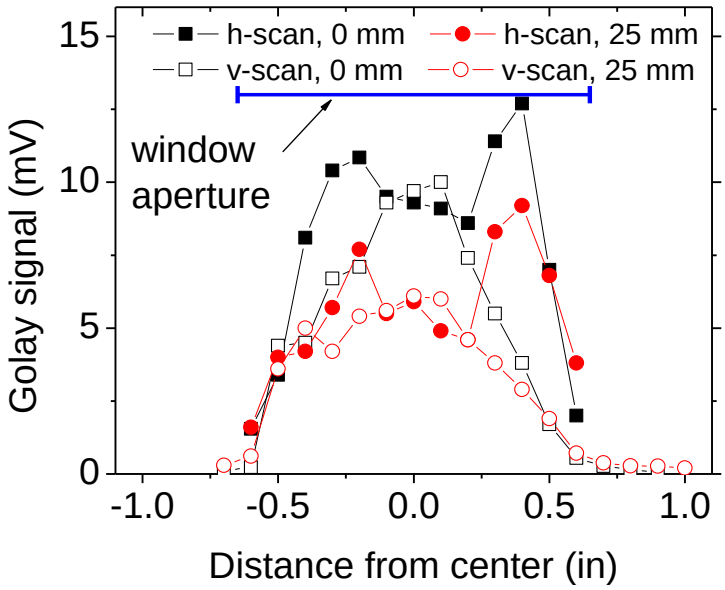

Figure 3.8 : TRION THz QCL vertical and horizontal beam profiles as a function of distance from cryostat window measured at two different positions. The black lines are the measured beam profiles in vertical (open square) and horizontal (solid square) directions near the cryostat window, whereas the red lines (open dot: vertical and solid dot: horizontal) are the same at a distance of 2.5 cm from the window.

A high-resolution emission spectrum (Fig. 3.9) was collected using a Fourier spectrometer (Bomem DA8). The QCL was excited at a current of 1.2 A for a 5 μs pulse durations at 3 kHz rep rate. The laser line width is seen to be 0.1 cm^{-1}, due to temperature induced shift during the laser pulse. Single mode emission is undesirable for ICLAS, so one should operate the laser closer to threshold, at lower current and shorter pulse duration. The spectrum, taken with a room temperature DTGS pyroelectric detector, has good signal-to-noise ratio. A simple, inexpensive, room temperature pyroelectric detector can be used instead of a Golay or 4 K bolometer.

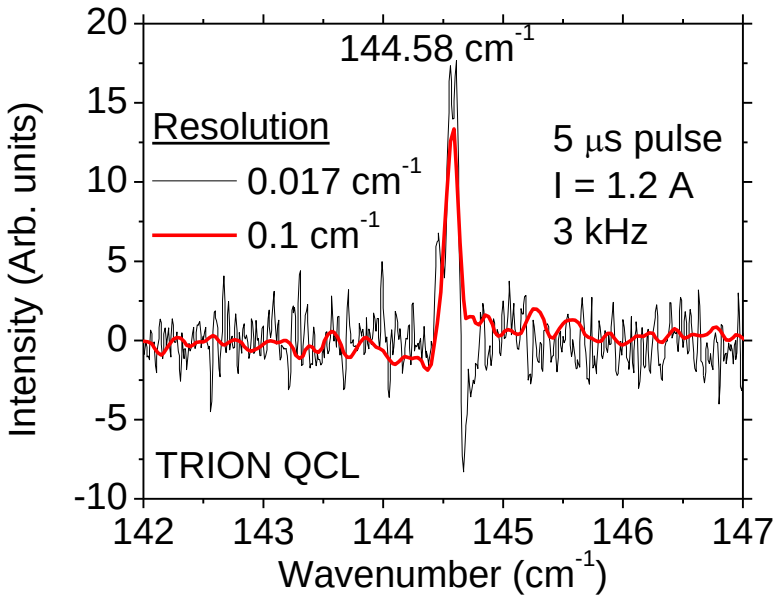

Figure 3.9 : High resolution emission spectrum of TRION THz QCL measured at a current of 1.2 A for a 5 μs pulse durations at 3 kHz rep rate.

After the external cavity laser, the next required enabling technology for a THz ICLAS system is a high-resolution real-time means of monitoring the emission spectrum. We consider a scanning central-fringe Fabry-Perot interferometer to be the most attractive option. To operate at 69.9 μm wavelength, requires a minimum FP translation of at least 35 μm to catch at least one resonance. We had used a translation stage controlled by Labview, and the DC output of the lock-in was recorded as a function of stage position (Fig. 3.10).

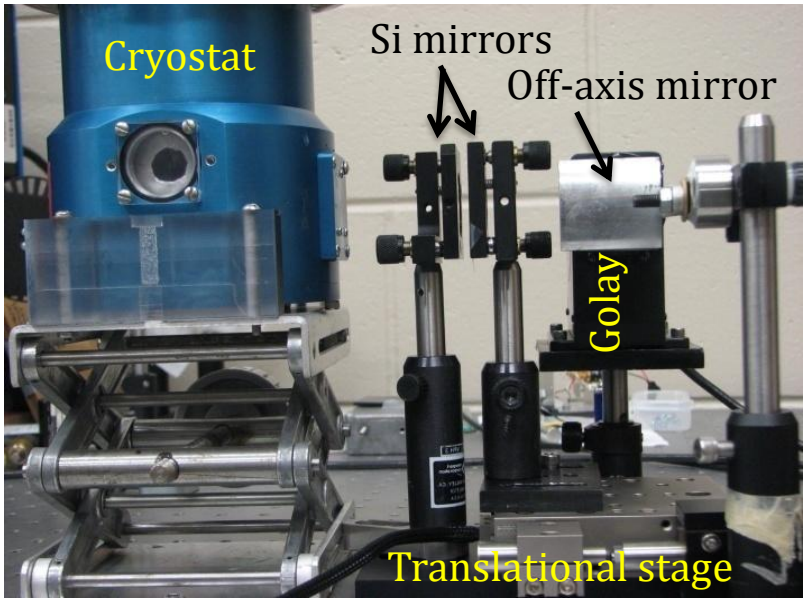

Figure 3.10 THz Fabry-Perot set up. From left to right, the THz QCL is mounted in the cryostat with internal collimating optics and a polyethylene window. A fixed mirror faces a moving mirror which is mounted to a motorized precision translation stage. An off-axis parabolic mirror directs the light to the Golay cell.

Fig. 3.11 presents the resonances obtained using the 69.9 μm wavelength QCL and double side polished (DSP) silicon wafers as the FP mirrors. The expected reflectivity for these mirrors is only $R = \left[\frac{n-1}{n+1}\right]^2$ = 30.0% considering the refractive index of silicon as 3.4. The measured finesse from Fig. 3.11 and Eq. 2.12 gives R = 31%, in very good agreement with expectations. Metal mesh mirrors with higher reflectivity will increase the finesse and resolving power of this instrument.

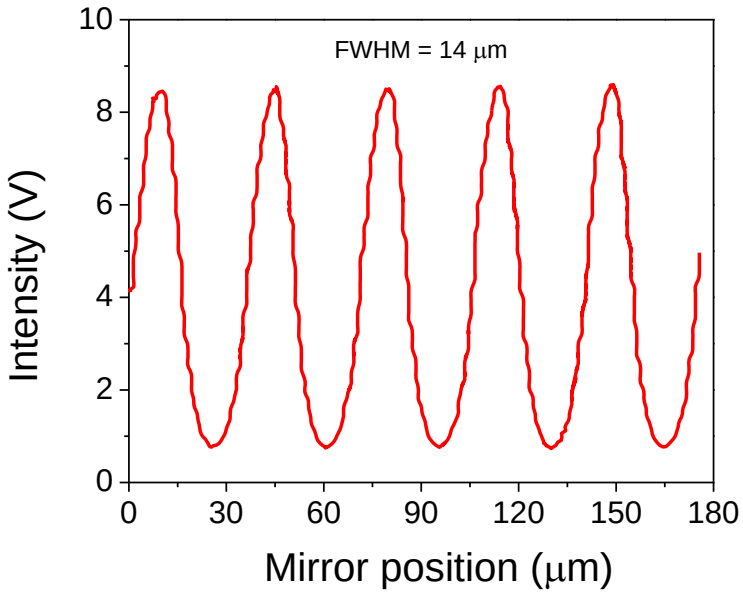

Figure 3.11 : Fabry-Perot spectrum of THz QCL measured with the setup shown in Fig 3.10. The measured FWHM is 14 μm.

3.4 Conclusion

Implementation of a THz QCL-based ICLAS system is complicated by the requirement for a cryostat to house the laser. This greatly restricts the working space, and the cryostat window introduces a loss element into the cavity. There is very strong interference from water vapor, and the molecular absorption cross sections for the type of vibration likely to occur in the THz are very low due to small dipole moments for such low frequency motions [5]. Currently lots of work has been done to increase the THz QCL operating temperature. People succeeded operating THz QCL at 186 K in pulse mode [54] and at 117 K in CW mode [55] using double plasmon metal-metal waveguide. This will eventually ease the difficulties of making THz QCL ICLAS system in near future.

CHAPTER 4: MID-IR EXTERNAL CAVITY QCL AT 9.38 μm

4.1 Introduction

Molecules have characteristic absorption features in the 3 - 12 μm wavelength range. This mid-IR molecular fingerprint region has remained largely unexplored by the ICLAS technique. Such a technique in mid-IR range would have broad application in defense, security, environmental monitoring, medical diagnostics, etc. Commercial QCLs that operate at pulsed mode and CW at room temperature, with a broad gain spectrum, are promising for ICLAS. In this chapter we describe a mid-IR ICLAS system based on an external-cavity, broadband, multimode, mid-IR quantum cascade laser at 9.38 μm.

4.2 Experiment

Fig. 4.1 presents a schematic of a stable confocal cavity consisting of two 90^{o} off axis gold coated parabolic mirrors of 2.5 cm focal length and two flat mirrors placed at a distances of L_1 and L_3 from the optical center of the parabolic mirrors. The QCL was placed at the common focal point of the two parabolic mirrors. A He-Ne laser was used to align the whole system before inserting the QCL. A small hole of diameter 0.15 cm in the middle of the first flat mirror outcoupled laser emission from the cavity into the FTIR spectrometer.

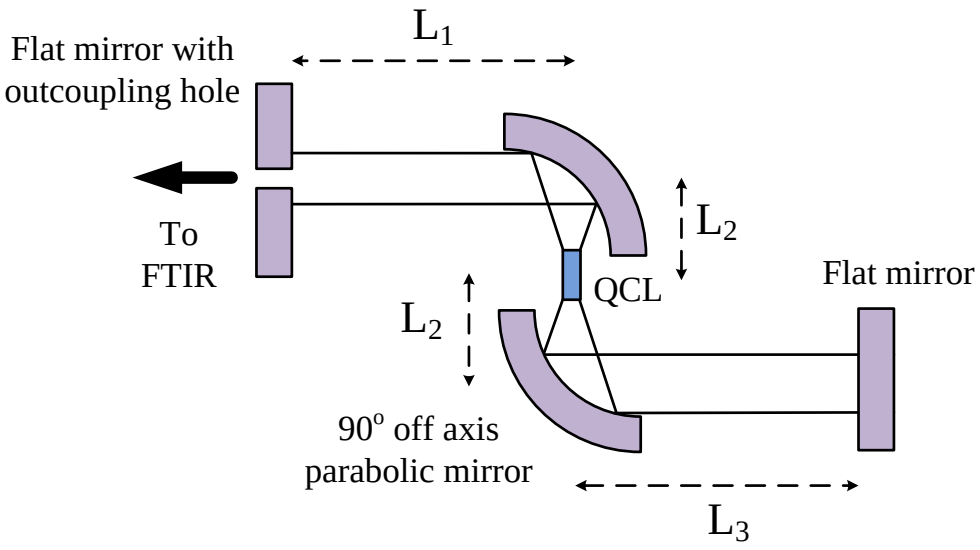

Figure 4.1 : Schematic of a Mid-IR QCL external cavity at 9.38 μm.

Fig. 4.2 presents the overall multimode laser emission spectrum of the 9.38 μm QCL measured with the Fourier spectrometer. The laser was excited at a feeding current of 1.8 A, 100 ns pulse duration and 10 μs rep rate at room temperature. The spectral emission width spans 60 cm^{-1}. The longitudinal mode separation of ~ 1 cm^{-1} is defined by the distance between the end facets of the QCL and its refractive index. Fig. 4.3 presents a high-resolution spectrum of the laser emission with the external cavity. With the external cavity, a mode fine structure appeared indicating the successful implementation of the external cavity.

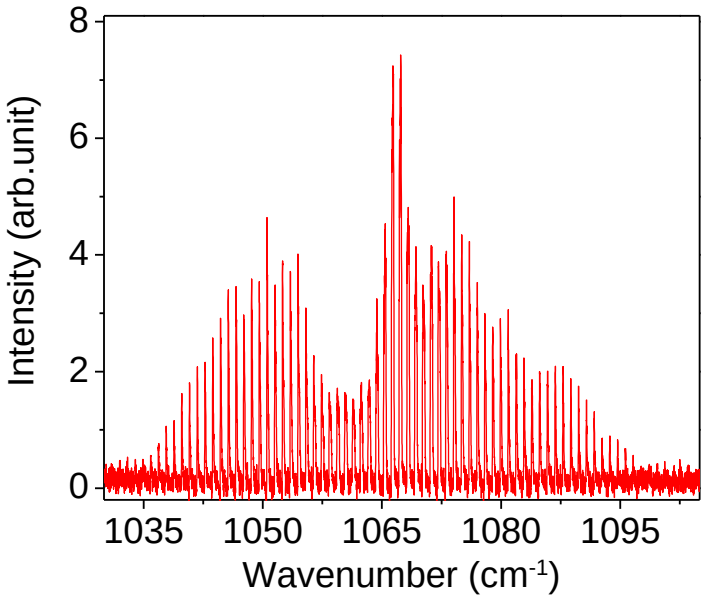

Figure 4.2 : Emission spectrum of a 9.38 μm multimode QCL measured by FTIR spectrometer.

Closer inspection of the mode fine structure is presented in the inset of Fig. 4.3, which reveals a mode spacing of ~0.05 cm^{-1}. In Fig. 4.1 schematic, L_1 = 6.95 cm, L_2 = 2.5 cm, and L_3 = 6.75 cm. A mode separation of 0.05 cm^{-1} corresponds to a total cavity length of ~ 9.25 cm, which is just half the (L_2 + L_3) of the external cavity length. For the ICLAS application, it is necessary to fill the entire spectral space of interest with external cavity modes. This goal is impeded by the mode structure of the active crystal itself as seen in Fig. 4.3. Thus, we realized the requirement of anti-reflection (AR) coatings on the end facets of the laser or a laser with end facets cut and polished at Brewster's angle.

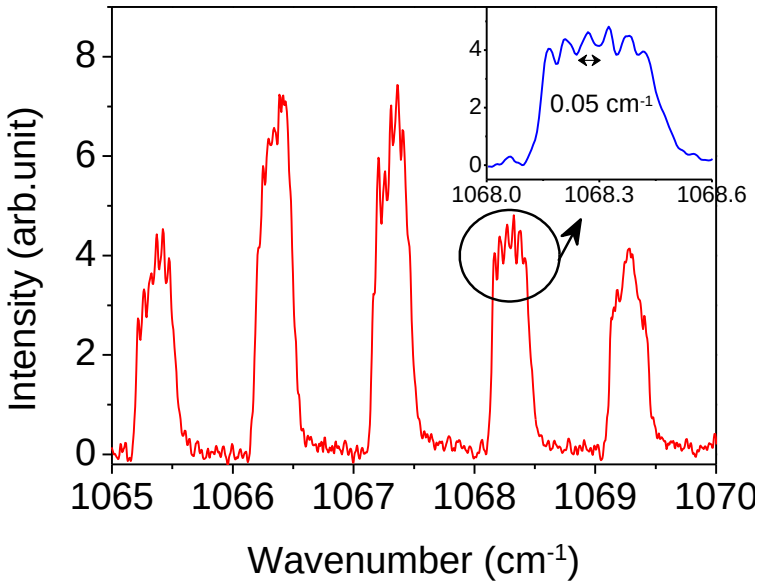

Figure 4.3 : High resolution spectrum of external cavity laser modes. The inset demonstrates a mode spacing of 0.05 cm^{-1}, which corresponds to a cavity length of ~9.25 cm.

4.3 Fabry-Perot Analyzer

Next in the level of importance to the ICLAS device concept is a compact means of determining the laser spectrum in real time. We have selected a high-resolution Fabry-Perot interferometer for this purpose. We require the finesse to be highest at our 9.38 µm wavelength. The FP transmission resonance needs to move over the emission bandwidth of QCL. This range is 9.524 to 9.302 µm wavelength. The Free Spectral Range (FSR) thus has to be at least 0.222 µm. That implies a maximum resonance order of about k = $\lambda/_{FSR}$ = 42, or a maximum mirror separation = $k\lambda/_2$ = 0.198 mm. This mirror separation has to be tuned over $dx = k\,d\lambda/_2$ = 42*(0.222)/2 = 4.7 µm in order to cover the full FSR. The feature we are looking for in that

range is expected to have a minimum linewidth of about 0.2 cm^{-1}, or 1.8 nm at our center wavelength. The necessary resolving power is $Q = \lambda/\Delta\lambda$ = 9400 nm/1.8 nm = 5222. Given the maximum resonance order, this implies a required minimum finesse of about $F = Q/k$ = 124. Reflectivity of the FP mirrors, from Eq. 2.12, gives R = 97.5%, which is needed at 9.38 μm ± 0.1 μm wavelength, i.e. 1% bandwidth. We used wedged ZnSe mirrors with AR coated at 9.3-9.5 μm on one side only, while the other side is HR coated with reflectivity > 97.5%.

Fig. 4.4 presents a photograph of the Fabry-Perot interferometer. One of the mirrors was fixed, while the other was placed in a mount with high-precision 3-axis alignment and piezo drivers. The piezo was controlled by a three-channel piezo driver. The 9.38 μm QCL was installed in the focus of the 90° off-axis parabolic mirror, which provided a collimated beam for the FP spectrometer. The signal transmitted by the FP was detected by a 77 K HgCdTe detector and was synchronously amplified. A linear ramp voltage of 0-10 V at a rep rate of ~10 Hz controlled the piezo driver for the FP.

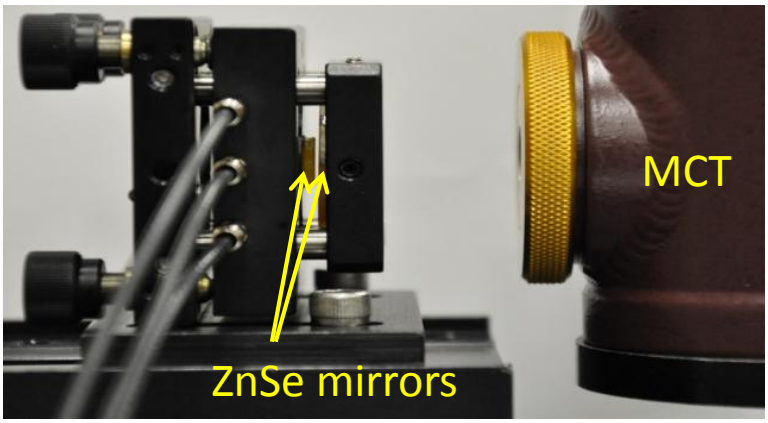

Figure 4.4 : Picture of the Fabry-Perot interferometer. The MCT detector appears to the right.

The signal transmitted by the FP vs mirror displacement is presented in Fig. 4.5 when the laser was operated under narrow band conditions. The spectrum corresponds to the 78th order of resonance. The spectrum was compared with the one obtained using a Fourier spectrometer (KBr beamsplitter, 77K HgCdTe detector) at a resolution of 0.017 cm^{-1} showing good agreement. A similar experiment was done with the same laser operated under broadband conditions, which is necessary for ICLAS. The best compromise between free-spectral range and resolution was found at 25th resonance order (Fig. 4.6), when the different resonance orders just start to overlap, while individual modes are still resolved. This spectrum compares well with the high- resolution spectrum obtained with the Fourier spectrometer. The achieved resolution is better than 0.5 cm^{-1}, which suffices for the expected pressure broadened vapor linewidths of at least 0.2 cm^{-1}.

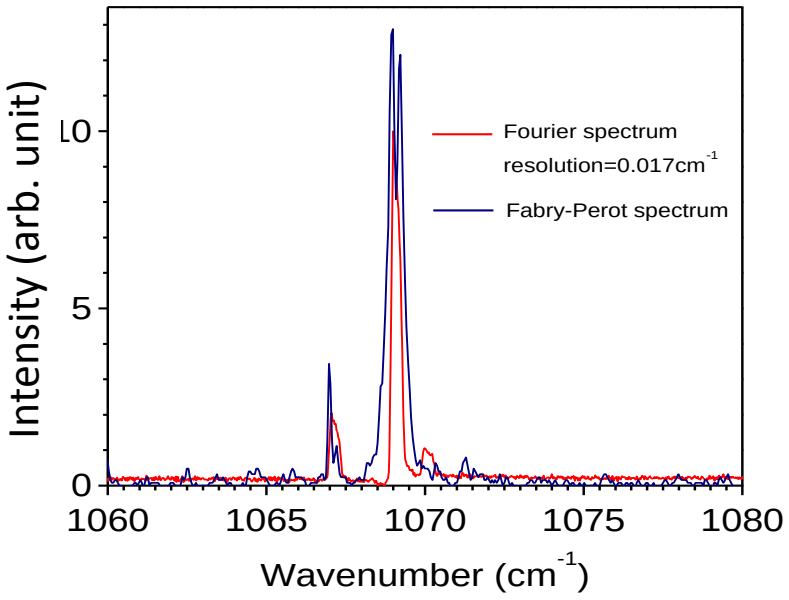

Figure 4.5 : Comparison of narrow-band QCL spectrum measured on Fabry-Perot and Fourier spectrometer.

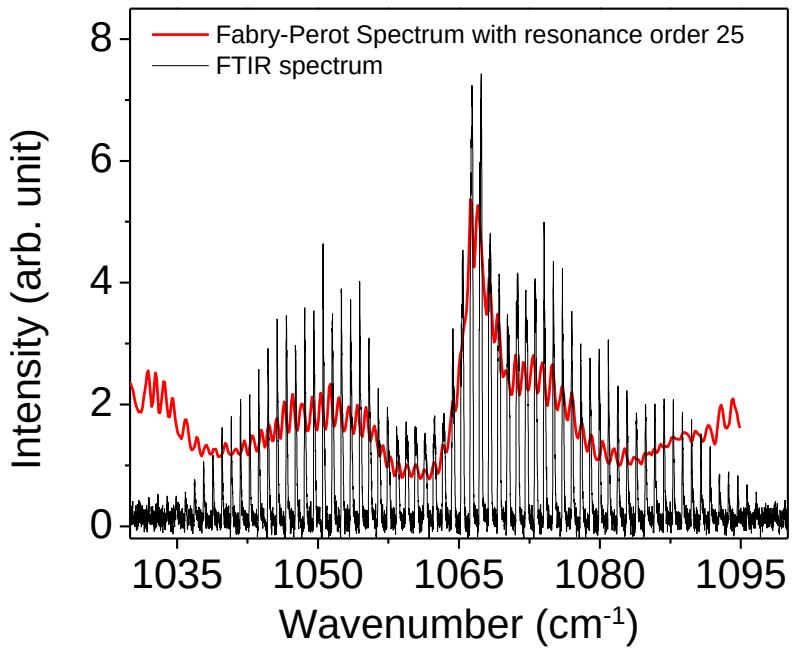

Figure 4.6 : Comparison of broadband QCL spectrum measured on Fabry-Perot and Fourier spectrometer. The Fabry-Perot spectrum corresponds to the 25th order of resonance.

4.4 Conclusion

A Mid-IR QCL external cavity at 9.38 μm is implemented. Fine mode structures from the external cavity operation are measured by FTIR spectrometer with a mode spacing of 0.05 cm^{-1}. To fill the entire spectral space by the external cavity modes, the QCL needs AR coating. A high resolution Fabry-Perot analyzer shows a resolution better than 0.5 cm^{-1}, which suffices for the expected pressure broadened vapor line widths of at least 0.2 cm^{-1}.

CHAPTER 5: MID-IR EXTERNAL CAVITY QCL AT 8.1 μm

5.1 Introduction

We realized that AR coating is an essential requirement for an external cavity QCL operation to fill the entire spectral space of interest with external cavity modes. As a second phase development process, we used an 8.1 μm QCL from Maxion with one end facet high-reflection (HR) coated and the other facet AR coated. The sensitivity of such a system can be enhanced by operating the QCL at longer pulse duration, preferably at CW mode.

5.2 Experiment

The measured threshold current of the QCL for a 2 ms pulse duration was 750 mA. The maximum duty cycle, the laser can withstand was 30% at room temperature. A schematic of the external cavity QCL configuration with an 8.1 μm QCL is shown in Fig 5.1. The QCL was installed at the focal point of a 90^{o} off axis gold coated parabolic mirror of focal length 2.5 cm. A flat mirror with an outcoupling aperture and the high reflecting end facet of the QCL formed the cavity. The system was initially aligned with a He-Ne laser. For this configuration the laser was never operated below room temperature.

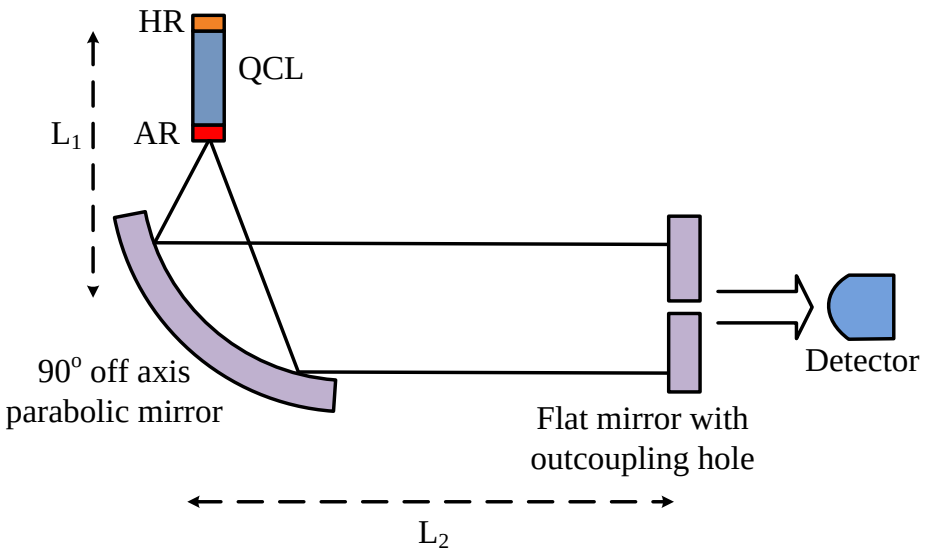

Figure 5.1 : Schematic of an external cavity QCL at 8.1 µm. The signal transmitted through the outcoupling hole is measured by a 77 K HgCdTe detector.

The QCL wavelength was chosen to coincide with the 8.1 µm absorption band of acetone. This solvent has high vapor pressure, which is favorable for a first vapor-detection demonstration and subsequent system optimization. Fig. 5.2 compares the transmission spectrum of acetone vapor, measured at a pressure of a few Torr in a 10 cm gas cell [5], to a low-resolution emission spectrum of the external-cavity QCL. The QCL was excited at 790 mA current, 100 ns pulse duration and 10 Hz rep rate. Both spectra were collected using a Bomem DA8 Fourier spectrometer. Though the laser operates on the shoulder of the band, where the absorption is considerably weaker, it is sufficient to demonstrate detection of acetone vapor, as shown below.

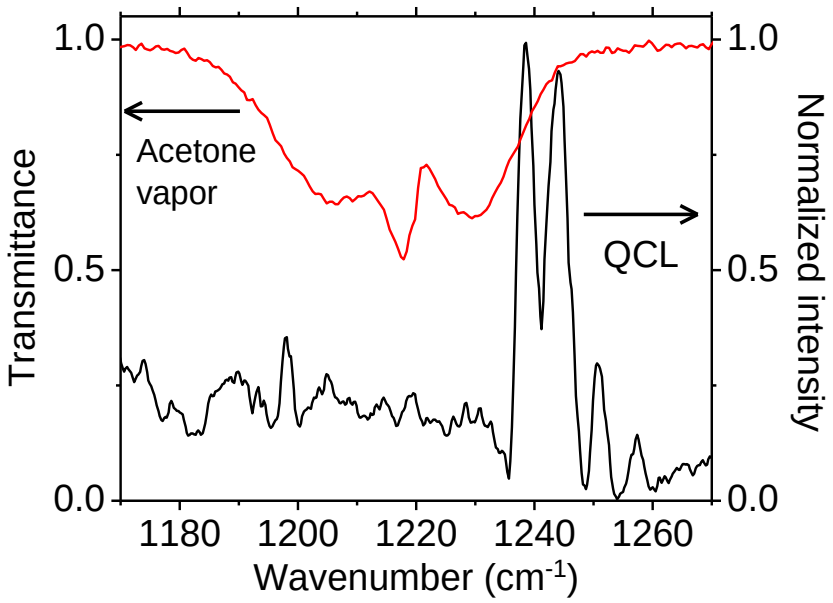

Figure 5.2 : Transmission spectrum of acetone vapor (red) measured at a 10 cm gas cell and at a pressure of 6 Torr at room temperature. The 8.1 μm QCL emission spectrum measured by FTIR is shown by the black line.

5.3 External Cavity Sensing Demonstration

The external cavity mirror was located ~ (L_1 + L_2) = 33 cm from the HR facet of the QCL. The gold coated mirror had a hole at its center for output coupling to the 77 K HgCdTe detector. When the alignment was right, the laser started to oscillate, the detector saturated, and the beam was found to be collimated with a diameter of about 1 cm.

Fig. 5.3 presents the effects of various absorbers on the total laser intensity. The laser was operated near threshold (790 mA) and an excitation pulse of 800 μs and at 10 Hz rep rate. The detector was initially saturated, but the emission intensity dropped as the laser chip was being heated due to the drive current.

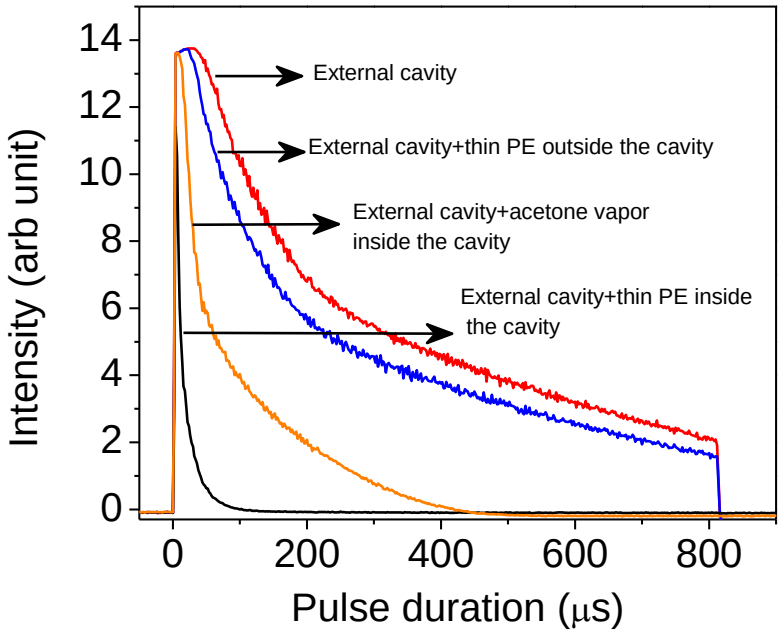

Figure 5.3 : Oscilloscope traces showing effects on recorded laser intensity of extra- and intra-cavity absorption.

When a polyethylene (PE) sheet was placed in front of the detector but external to the cavity, the signal dropped by ~10% due to single pass absorption by the PE. However, when the PE sheet was placed inside the cavity, the lasing was almost completely extinguished. The signal with acetone vapor inside the cavity was also strongly attenuated, though by less. These results show that an intracavity absorber with 10% single pass loss causes nearly complete laser extinction. Similarly, unsaturated acetone vapor weakly confined in a ~ 10 cm cell also gave a nearly complete laser extinction. From Figs. 5.2 and 5.3, we estimate the unsaturated vapor pressure of acetone to have been ~ 1 Torr. The projected sensitivity limit for acetone vapor based on the

attenuation of the total power using this set-up is ~ 0.1 Torr. Based on observed laser intensity variations using our pulsed QCL driver, we estimate that the sensitivity can be increased to ~ 10^{-4} Torr using a more stable laser driver designed for longer pulse operation. Further increases in sensitivity can be obtained when the sensing is based on the changes to the laser emission spectrum rather than emission power. Additional sensitivity increases can be obtained by operating the laser continuous wave (CW) rather than pulsed, which substantially increases the effective IR path length.

5.4 High resolution spectroscopy of external cavity configuration

High resolution spectroscopy was performed using the Fourier spectrometer to see the fine mode spectrum expected of the external cavity configuration. The laser was operated using an ultra-stable laser driver (ILX Lightwave, LDX3232). Fig. 5.4 presents the obtained spectrum when the laser was excited at 875 mA current, 2 ms pulse duration and 10 Hz rep rate. The lower frequency structure of the spectrum presented in Fig. 5.4 shows clear evidence of periodic mode structure with mode separation of 0.55 cm^{-1}. This structure arises due to feedback reflections from the output facet of the QCL chip. However, due to the AR coating on this facet, this structure practically vanishes on the high frequency side of the emission. The expected mode separation for the cold 33 cm long external cavity for this experiment is 0.015 cm^{-1}. Despite the close match of the best spectrometer resolution of 0.017 cm^{-1}, these modes were unresolved in Fig. 5.4 due to existence of multiple higher order transverse modes. However, installation of a 10 mm diaphragm within the cavity causes the fine mode structure to appear by

extinguishing the higher order transverse modes. Fig. 5.5 presents a detail of the spectrum on the low-wavenumber shoulder of the emission spectrum. One sees a regular periodic pattern of modes characterized by strong single peaks separated by slightly weaker double peaks. The observed fine mode structure includes typical mode spacing of 0.03 cm^{-1}, corresponding to even modes of the cold resonator.

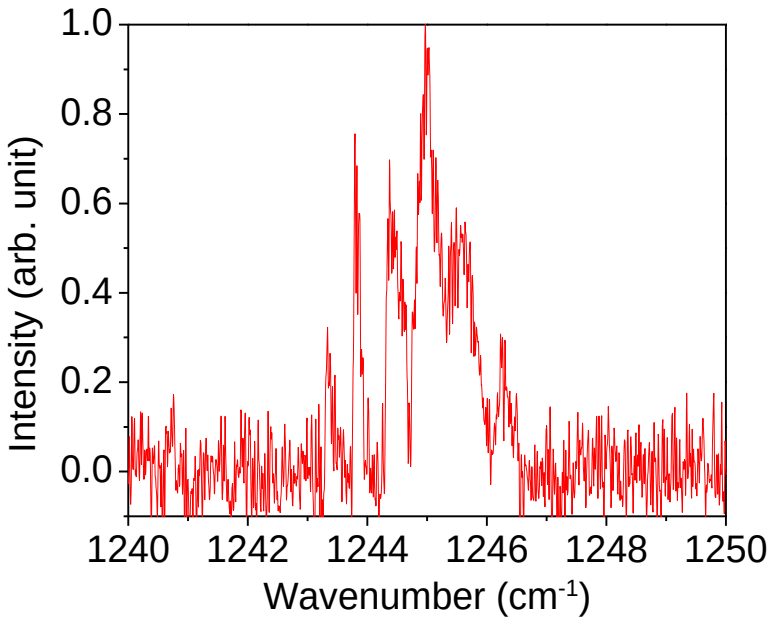

Figure 5.4 : Emission spectrum of 8.1 μm QCL with external cavity. The laser was excited at 875 mA current, 2 ms pulse duration and 10 Hz rep rate. The spectral resolution was 0.017 cm^{-1}.

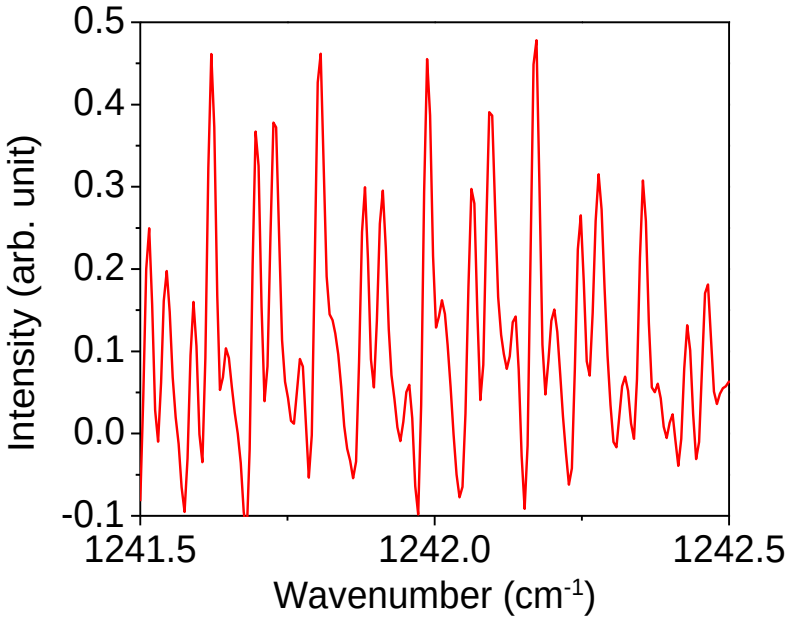

Figure 5.5 : Fragment of high-resolution 8.1 μm QCL external cavity mode structure under the same operating conditions but with the addition of a 10 mm intracavity diaphragm.

5.5 Effect of intracavity elements on the system performance

Fig. 5.6 presents the effect on the high resolution spectrum when a high purity 1 mm thick Si spacer was placed inside the cavity. The laser was operated at the same operating conditions as mentioned in the previous section. The laser still worked despite the ~ 20% losses due to reflection from the Si surfaces. Laser operation showed little sensitivity to the exact orientation of the Si spacer with respect to the beam. This showed that the reflected radiation was not coupled back into the laser active medium. Moreover the maximum emission output was observed at slight disorientation of the silicon spacer from the cavity optical axis. Strong mode selection caused by Fabry-Perot interference inside the Si etalon indicates fast development of

mode competition, which is critical parameter for sensitivity of the intracavity laser spectrometer. In other words, even though the period of FP transmission modulation of the Si spacer was rather wide (~ 1.3 cm^{-1}), small differences in transmission of close laser modes separated by ~ 0.03 cm^{-1} was sufficient to suppress all neighboring modes, leaving only 1-2 dominating modes in the center (Fig. 5.7).

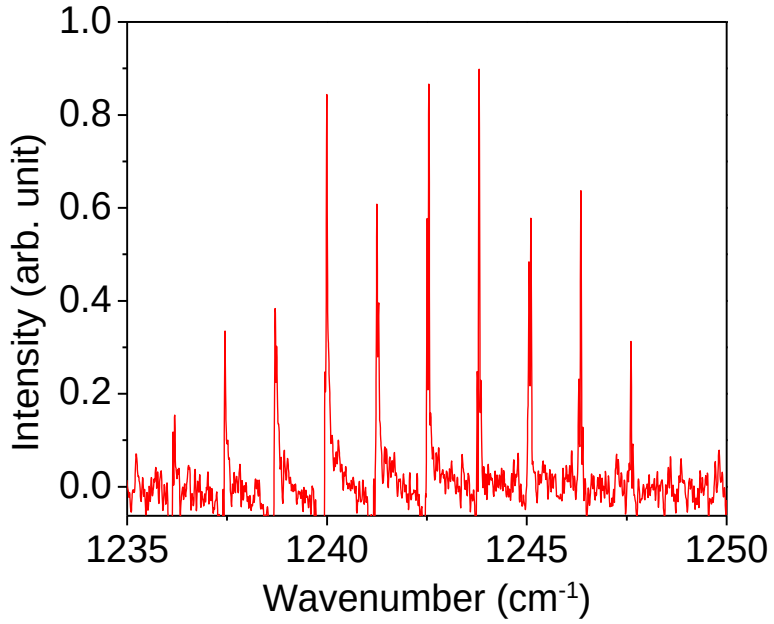

Figure 5.6 : High resolution emission spectra for the laser with external cavity with intracavity Si spacer.

Consequently, even the low finesse of a silicon flat (~ 8) suffices to select the laser wavelength with an active cavity resolving power *Q* of order ~ 1200 cm^{-1}/0.03 cm^{-1} = 40000. The *Q* of the 1 mm thick passive silicon flat itself is only 850. This is promising for the potential of achieving high Q tunable wavelength selection and tuning with an intracavity scanning FP.

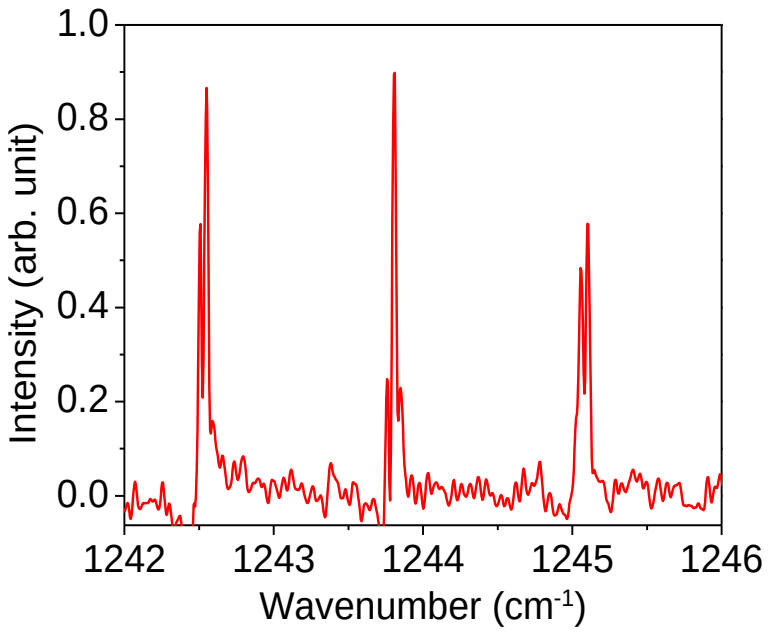

Figure 5.7 : Fragment of high resolution emission spectrum with intracavity Si etalon. Spacing between frequency separation bands is 1.3 cm^{-1}. Individual fine structure mode separation is ~0.03 cm^{-1}.

Demonstration of the system operation with intracavity Si window has the following significance: 1) It must be possible to use normal incidence (as opposed to Brewster angled) windows for an intracavity gas cell, if the window is thick enough to allow FP resonances to be ignored, or if it has AR coatings, or if it is wedged and has AR coatings. 2) It should be feasible to install piezo FP interferometer inside the cavity to achieve a continuously tunable single mode laser. Such, may be competitive with usual grating tuned external cavity QCL designs.

5.6 Conclusion

An external cavity QCL at 8.1 μm with one facet AR coated and the other facet HR coated is demonstrated here. The effects of various absorbers on the total laser intensity is demonstrated. The unsaturated vapor pressure of acetone measured by this external cavity configuration is ~ 1 Torr. The sensitivity limit for acetone based on the attenuation of the total power inside the cavity is found to be ~ 0.1 Torr. A fine mode structure of mode spacing ~ 0.03 cm^{-1}, corresponding to even modes of the cold resonator is observed. The effect of an intracavity Si spacer on the system allows to use normal incidence gas cell inside the cavity. It also allows to install piezo FP interferometer inside the cavity to achieve a continuously tunable single mode laser.

CHAPTER 6: SENSITIVITY TO ACETONE VAPOR

6.1 Introduction

The stability and sensitivity of sensing of the external cavity QCL system can be greatly enhanced by operating the QCL at CW mode. This requires the QCL to be cooled below the room temperature. The cooling also reduces the threshold current. This chapter presents the sensitivity of the 8.1 μm QCL ICLAS system when the QCL was operated at CW mode in the presence of acetone vapor.

6.2 Experiment

To operate the QCL at CW mode, it was installed on a water cooled mount. A temperature sensor was installed on the surface of the mount close to the QCL to monitor the temperature. The ultimate temperature measured on the surface of the mount was 14^{o} C, though the QCL chip temperature was believed to be a little bit higher than 14^{o} C because of constant driving current across the chip.

For first vapor-detection demonstration and subsequent system optimization we selected acetone as the target vapor, since this solvent has high vapor pressure and a well-established spectrum [5]. The schematic of the external cavity configuration for the 8.1 μm wavelength QCL is presented in Fig. 6.1. Laser emission and acetone absorption spectroscopy were

performed using a Bomem DA8 Fourier spectrometer with globar source, KBr beamsplitter, and 77 K HgCdTe detector.

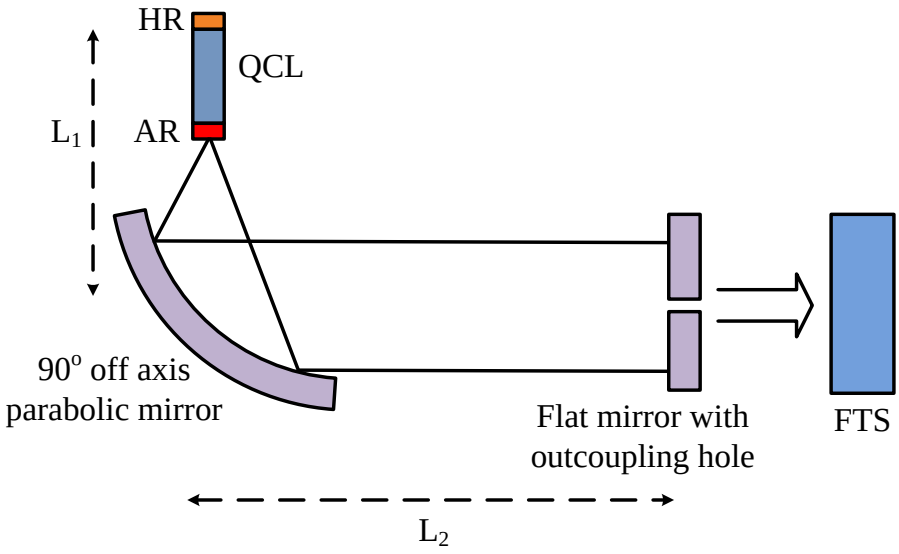

Figure 6.1 : Schematic of an external cavity QCL at 8.1 μm. The transmitted spectrum of the external cavity was measured using Fourier spectrometer (FTS).

6.3 Results

Fig. 5.2 in the previous chapter compares the transmission spectrum of acetone to an emission spectrum of the external-cavity QCL. The acetone was measured at a pressure of 6 Torr in a 10 cm gas cell [5]. The acetone absorption varies monotonically across the 1230 to 1260 cm^{-1} (7.93 to 8.13 μm wavelength) gain band of the QCL. The laser was operated in short pulse mode (100 ns) to obtain a broad emission spectrum. A high-resolution spectrum measured

at the resolution limit of the spectrometer (0.017 cm^{-1}) revealed the fine structure with individual mode separation of ~0.03 cm^{-1} due to the longitudinal modes of the external cavity.

When the laser was operated in CW mode, the broad laser emission spectrum collapses to just a few of the external cavity modes. Fig. 6.2 demonstrates how the CW laser emission spectrum reacts to the presence of acetone vapor inside the cavity. Though the laser threshold current was 920 mA at the ~14^{o} C operation temperature, the current was set to 940 mA to avoid instabilities arising from the temperature variation in the chip near threshold. The concentration of acetone vapor had been chosen below the level when remarkable drop of the laser intensity occurred. In this experiment the acetone concentration inside the open cavity could not be accurately quantified, but subjectively it was slightly above human nose sensitivity of ~41 ppm [56]. In response to the vapor, the laser emission shifted by 6 cm^{-1} away from the absorption toward higher frequencies, even to a region where no laser emission was previously observed. This behavior demonstrates the sensitive response of the system to frequency-dependent intracavity absorption.

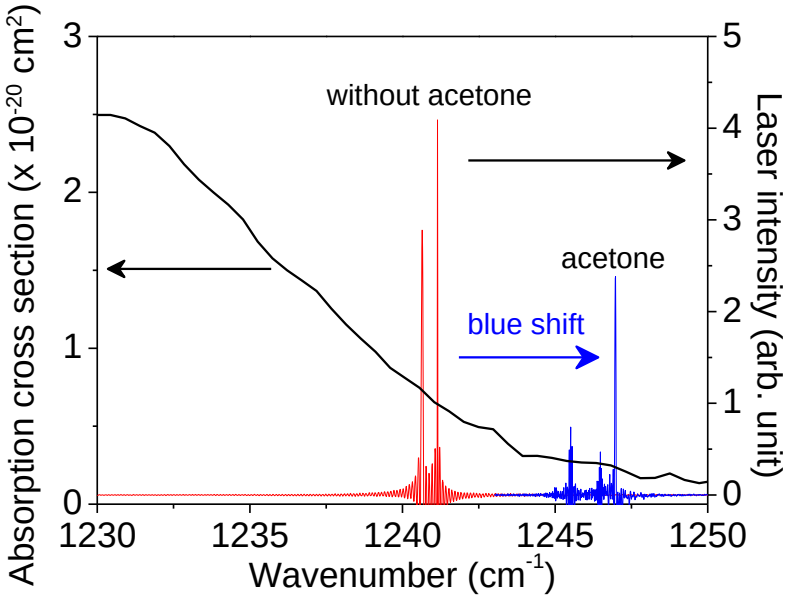

Figure 6.2 : Emission spectrum of the external cavity QCL together with absorption cross section of acetone. The QCL was operated at CW at 940 mA excitation current. The spectral resolution of the spectrometer was 0.5 cm^{-1}. Two separate laser spectra are plotted, one without, and one with acetone vapor in the cavity. When the open laser cavity is exposed to acetone vapor, the spectrum blue shifts, as indicated by the arrow

Numerical solution of the laser rate equations (Eqs. 2.6 and 2.7) determines the temporal evolution of the QCL emission spectrum. The spectrum of the acetone absorption cross section σ taken from [5] was fit to a 2nd order polynomial to obtain a smooth function for the calculations. The cross-section in the 1235-1250 cm^{-1} region decreased from 1.75 x 10^{-19} to 0.15 x 10^{-19} cm^2. The absorption coefficient α_q at the q-th laser mode was determined using $\alpha_q = n\ \sigma_q$, and the concentration n taken to be 5.4 x 10^{15} cm^{-3}, or ~ 200 ppm, which is consistent with subjective estimate made by smell. This corresponds to an acetone vapor pressure of 165 mTorr.

QCL parameters used in numerical simulation were either estimated or taken from the literature where available. The active layer length L of the QCL was taken to be 3 mm. We estimated a beam waist of 4 μm, which gave a cavity mode volume V_c = 3.7 x 10^{-8} cm^3. The value of the gain per round trip per unit time B_o was calculated using $B_o = c\sigma_s/V_c$, assuming a stimulated emission cross-section σ_s ~10^{-20} cm^2 (typical laser emission cross-section). The value of A was estimated as 7.1 x 10^6 s^{-1} assuming a spontaneous decay time τ_{sp} of 1.4 x 10^{-7} s [57]. The broadband cavity loss was obtained from $\gamma = -\frac{c}{2L} ln[R(1-T_i)^2]$ where T_i is the waveguide fractional loss per pass (due to diffraction, scattering, and absorption loss in the active medium), and R is the fractional cavity output coupler reflectivity [15]. Estimating reasonable values of T_i = 0.25 and R = 0.8, we found γ ~ 3.9 x 10^{10} s^{-1}. The normalized pump rate was taken as $\eta = P/P_{th}$ = 18, where P_{th} is the threshold pump rate, and the spectral width of the gain was Q (HWHM) = 4000 (120 cm^{-1}).

Fig. 6.3 shows the calculated laser emission spectrum without and with acetone inside the cavity. The spectra plotted correspond to an integration time of 52 μs from the beginning of the laser excitation. The plot clearly shows a 6 cm^{-1} shift toward higher wavenumbers, which is in agreement with the experiment.

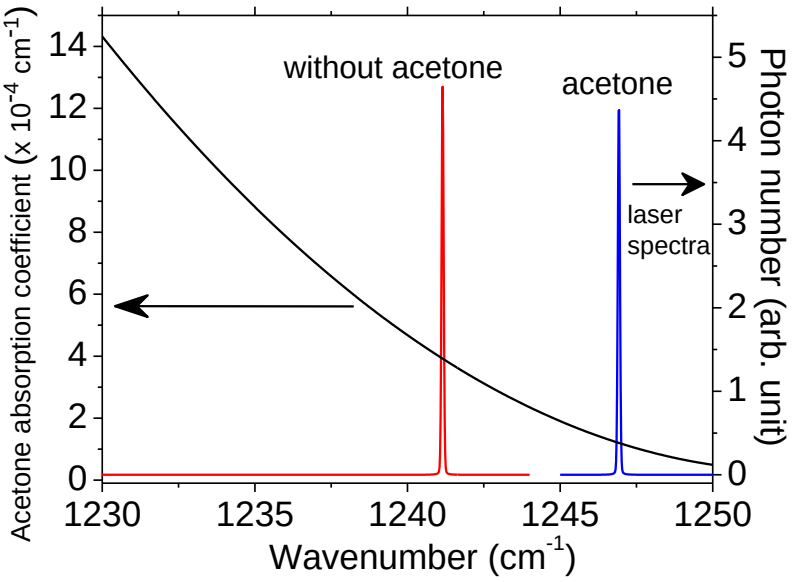

Figure 6.3 : Calculated laser emission spectra without (red) and with (blue) acetone vapor inside the cavity. The acetone profile was quadratic with a concentration of 5.4 x 10^{15} cm^{-3}, or 165 mTorr pressures. The spectrum with acetone shows a clear 6 cm^{-1} shift to higher wavenumbers.

6.4 Summary and Discussion

The response of the laser emission spectrum for an open cavity QCL to the intracavity absorption of acetone vapor at 8.1 μm wavelength is demonstrated. The laser emission spectrum shifts by 6 cm^{-1} towards higher frequency in presence of acetone vapor at an estimated partial pressure of 165 mTorr corresponding to ~200 ppm.

Assuming a minimum detectable shift of 0.03 cm^{-1}, which is the observed external cavity mode spacing, the sensitivity limit for acetone using the given set-up is estimated from similar

calculations to be ~320 ppb. This is improved somewhat to the value 240 ppb by (numerically) shifting the QCL emission wavelength closer to the peak of the acetone absorption.

CHAPTER 7: SENSITIVITY ESTIMATION OF ACETONE VAPOR USING FABRY-PEROT ANALYZER

7.1 Experiment

The experimental set up and details of the external cavity mid-IR QCL at 8.1 μm was described in Fig. 6.1. Fig 7.1 presents a schematic of the system with a FP analyzer. The FP was formed from a pair of ZnSe flats of 2 mm thickness, with high reflection coatings (97.5%) on the facing surfaces, and AR coatings on the outer surfaces. The flats were wedged (30-arcmin) to eliminate unwanted secondary FP resonances within the substrates themselves and to prevent reflections back into the cavity. The QCL output spectrum was coupled to the fixed FP through the aperture of the flat mirror forming the external cavity. The radiation transmitted by the FP was detected using a 77 K HgCdTe detector.

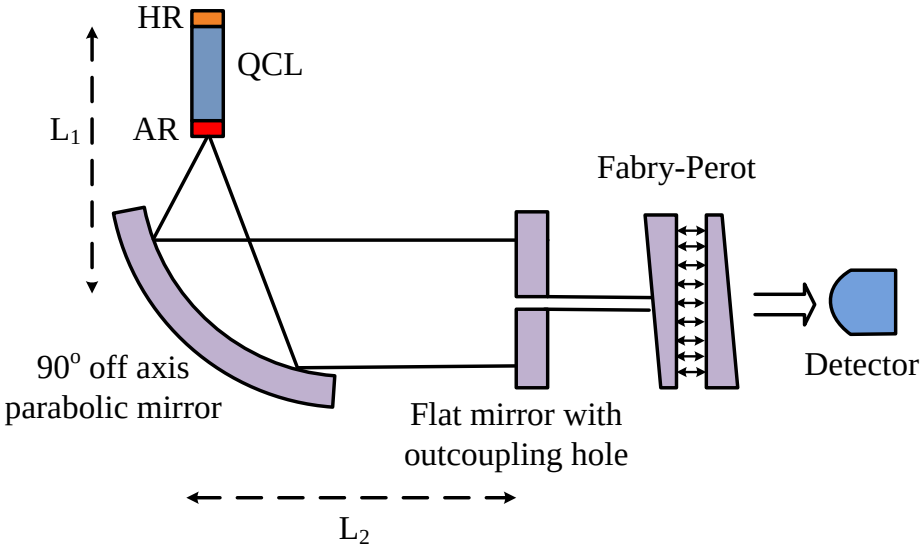

Figure 7.1 : Schematic of the 8.1 μm QCL external cavity system coupled with Fabry-Perot analyzer.

7.2 Results

Fig. 7.2 presents the transmission spectrum of the ZnSe flats along with the QCL emission spectrum measured by FTIR spectroscopy. The measured transmission spectrum of ZnSe confirmed the design-specified reflectivity of ~ 96.7% at our working QCL wavelength of 8.1 μm.

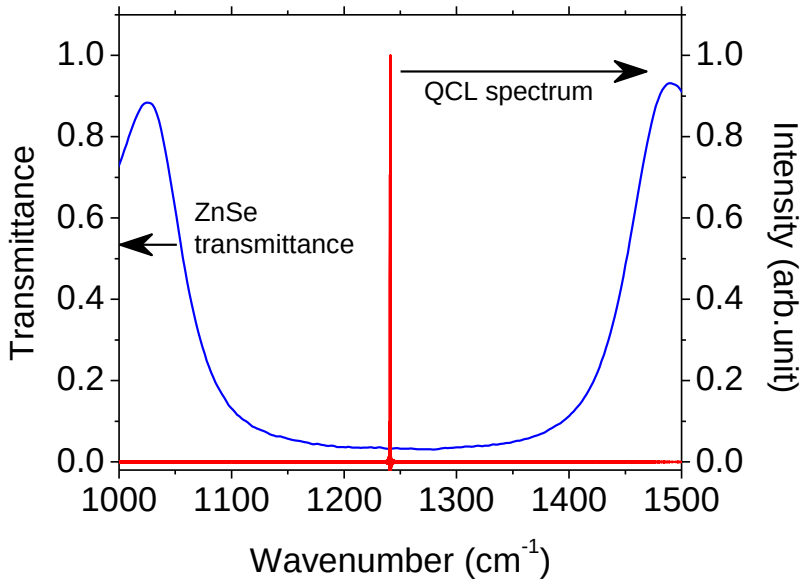

Figure 7.2 : Transmission spectrum of ZnSe mirror along with the emission spectrum of 8.1 μm QCL measured by FTIR.

The spectroscopy on the external cavity mid-IR QCL system showed that the emission spectrum stabilizes after ~1 ms of pulse duration. For shorter pulses, the spectrum was very unstable due to fast temperature rise in the active crystal, causing poor repeatability of the spectrum dynamics. After 1 ms, the spectrum stabilized but continued a slow adiabatic drift due

to the continued slow drift of the active chip temperature. This slow but stable shift of the emission spectrum was very repeatable from pulse to pulse, allowing us to monitor the mode spectrum as it passed through the narrow fixed transmission resonance of the FP. This also allowed the QCL to work at 5-10 ms pulse duration range, rather than at CW. The spectrum may be observed in real time on an oscilloscope.

In this configuration the system was found to be sensitive to water vapor in the ambient laboratory air. The QCL wavelength resides at the edge of the 8-12 micron "water window" as shown in Fig. 7.3. This transmission spectrum was measured at an effective optical path length of 2000 m at sea level [58]. The humidity at this level is ~ 75% [58]. The corresponding absorption coefficient in this window is from 5.5 x 10^{-6} cm^{-1} to 1.4 x 10^{-6} cm^{-1} [59]. The 8.1 μm QCL wavelength is shown as a red arrow in the figure. From this figure, we estimated the absorption coefficient of this outdoor air sample to be 4.1 x 10^{-6} cm^{-1}. This value was considered with extreme care and compared with literature value. Rather than a discrete absorption, the range of 8-12 μm wavelength in the atmosphere is considered as a water vapor continuum absorption coming from the wings of spectrally distant absorption lines of water vapor. The published value of the absorption coefficient in this range is ~ 1.35 x 10^{-6} cm^{-1} at a partial pressure of ~ 9.4 Torr and at 10 μm wavelength [60]. This partial pressure was close in value to that we have calculated from Fig. 7.3 at 8.1 μm. The HITRAN data also gives absorption coefficients of ~ 10^{-7} cm^{-1}. In the climate-controlled air of a laboratory, the humidity level is ~ 40-50%, which gives an absorption coefficient of 7 x 10^{-7} - 9 x 10^{-7} cm^{-1} at room temperature [60].

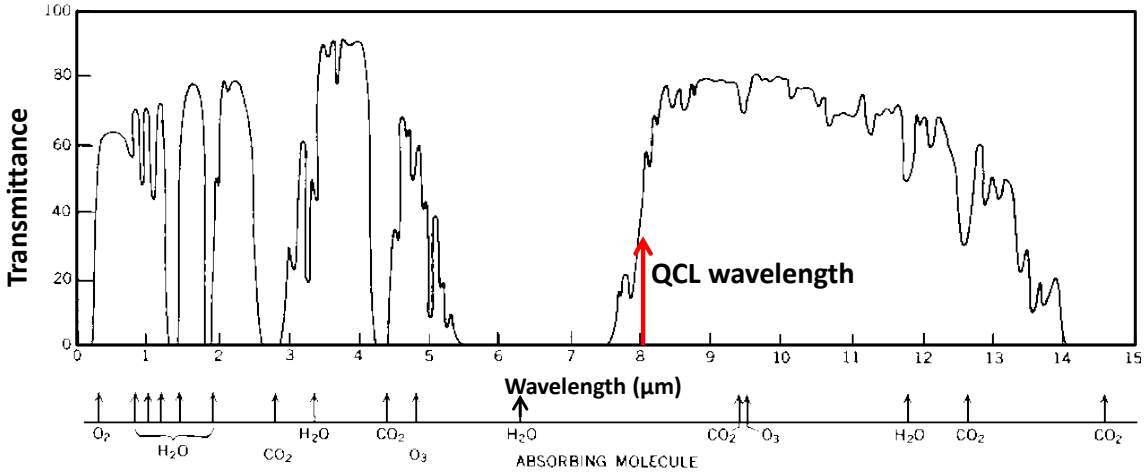

Figure 7.3 : Transmission spectrum of atmospheric air measured at sea level at an effective optical path length of 2000 m. From ref [59].

The 8.1 μm wavelength is on the short wavelength edge of the atmospheric absorption band (Fig. 7.3) whereas it is on the long wavelength side of acetone absorption (Fig. 5.2). When the laser cavity is purged with dry nitrogen, keeping the FP interferometer at fixed position, additional modes appeared on the higher frequency side of the spectrum. This confirmed the system is sensitive to laboratory humidity with an average absorption coefficient at the level of 8×10^{-7} cm^{-1}. Fig. 7.4 shows the oscilloscope trace, for which the time axis corresponds (non-linearly) to the emission wavelength due to the thermal drift of the laser spectrum through the narrow FP pass band. The QCL was excited at 940 mA current for a pulse duration of 5 ms and 5% duty cycle.

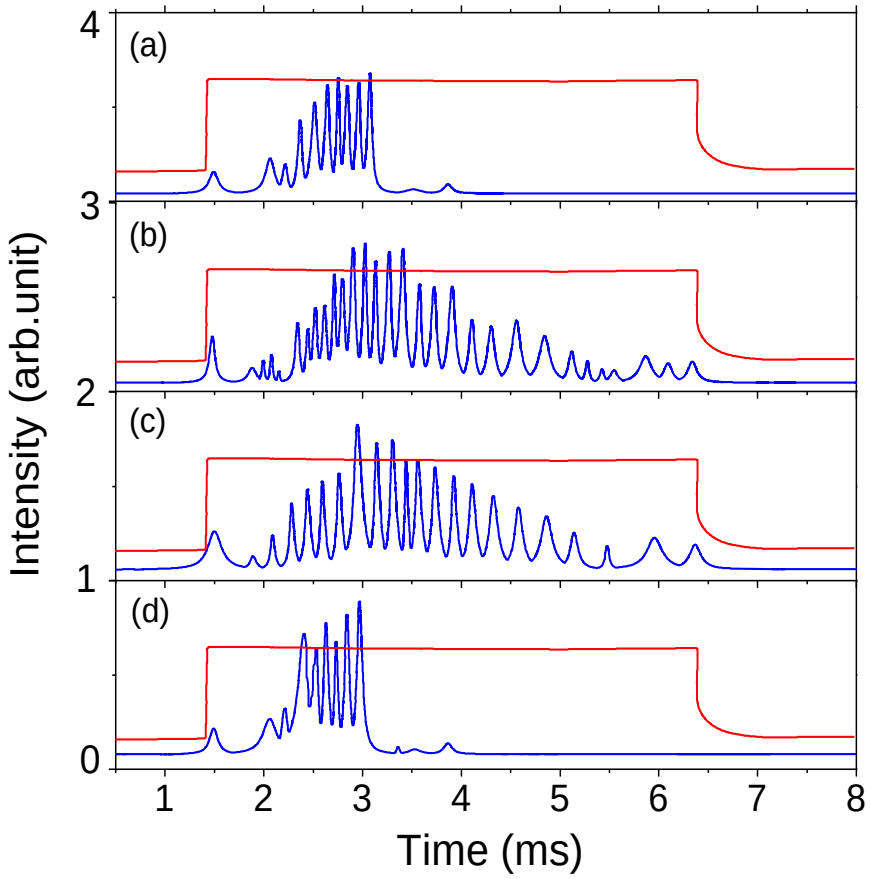

Figure 7.4 : Oscilloscope traces of the spectral dynamics of the external cavity configuration. (a) appearance of the mode in the beginning of the pulse when the cavity was filled with lab air (b) new modes appear in the higher frequency side when the cavity was purged with dry nitrogen. The QCL was excited slightly above the threshold current at pulse duration of 5 ms and 5% duty cycle. The current profile in the active chip during the pulse is also shown by the square wave (red) in each plot. (c) stronger mode appearance at a later time (d) the modes went back to its original position when the cavity is reintroduced with lab air.

The modes were seen (Fig 7.4 (a)) in the beginning of the pulse when the cavity was filled with lab air. Purging the cavity with dry nitrogen causes 10-12 new modes to appear on the long wavelength side of the laser spectrum, even in a region where no modes were seen before. Fig

7.4 (b) and (c) shows the temporal evolution of the modes on the higher frequency side, at two different instantaneous time. The fundamental sensitivity limit of the system is thus easily defined by this demonstration. In reality the change in the absorption coefficient due to purging with N_2 was less than the normal 7 x 10^{-7} - 9 x 10^{-7} cm^{-1} for water vapor, by as much as a factor of 2-3, since the cavity was inefficiently tented to affect the purge. This would give an absorption coefficient change on purging of only 3 x 10^{-7} cm^{-1} or 111 ppm when mixed with standard air. This value is obtained by calculating the concentration of water vapor molecules assuming an absorption cross-section of ~ 10^{-22} cm^2 [60]. The laser spectrum went back to its original position (low frequency side) when room air was reintroduced (Fig 7.4 (d)) into the cavity.

The behavior of the cavity in presence of acetone vapor was similar to that depicted in Fig. 7.4 for purging with dry nitrogen, when all other parameters of the system were same. The absorption coefficient of acetone at saturated vapor pressure (180 Torr) is 1.25 cm^{-1} [5] at our working wavelength. We have demonstrated that the ICLAS system is sensitive to absorption coefficients as small as 3 x 10^{-7} cm^{-1} using water vapor at a concentration of $n_{H_2O} = 111$ ppm or $P_{H_2O} = 9.4$ Torr partial pressure. The minimum detectable concentration is inversely proportional to the absorption cross-section at the laser wavelength. We may estimate the sensitivity for other molecules using the relation $n\sigma = \left(n_{H_2O}\right)_{min}\sigma_{H_2O} = \alpha_{min} = 3$ x 10^{-7} cm^{-1}, or $n = \frac{\sigma_{H_2O}}{\sigma}\left(n_{H_2O}\right)_{min}$. From [5], for acetone at 8.1 μm, $\sigma = \frac{1.25\ cm^{-1}}{180\ Torr}kT$. For water, $\sigma_{H_2O} = \frac{3\times10^{-7}cm^{-1}}{9.4\ Torr}kT$. Then, the sensitivity limit for acetone would be $n = \frac{3\times10^{-7}}{9.4}\frac{180}{1.25}111$ ppm = 510 ppt. This fundamental behavior of the cavity in presence of dry nitrogen and acetone uniquely

defines the sensitivity of the system even for an unquantified marker if its absorption coefficient is known at that wavelength.

7.3 Conclusion

The sensitivity limit of an external cavity mid-IR QCL is estimated when the system is combined with a fixed Fabry-Perot interferometer. The estimated sensitivity is two orders of magnitude higher than the previously obtained value when the system was not coupled with Fabry-Perot interferometer. The cavity is highly sensitive to the presence of water vapor in air. The calculated absorption coefficient of water vapor is 3×10^{-7} cm^{-1} or 111 ppm. The behavior of the cavity in presence of dry nitrogen and acetone is same. The sensitivity obtain for acetone is 510 ppt. This fundamental behavior defines the sensitivity of the system even for the presence of an unquantified marker inside the cavity.

CHAPTER 8: ELCTRONICS AND SOFTWARE

To make a man portable and field deployable system, all the electronics needed to operate the various components of our ICLAS system have to be integrated into a single control box. We used a National Instrument compact RIO (cRIO) chassis, which is a small plug-in rack with an onboard processor running Labview. Laser driver, piezo controller for the Fabry-Perot, detector power supply and preamp are the three main components to be integrated into the cRIO.

The cRIO chassis employs a real time processor and Field Programmable Gate Array (FPGA) to provide true parallel processing with a real time clock. Plug in modules include the analog to digital (A/D) converter (NI 9223), digital to analog (D/A) converter (NI 9264), and an amplifier module for driving the piezo stages.

To drive the laser initially, we used an LDX-3232 high compliance current source from ILX Lightwave. This driver is bulky for our purpose, but it is a very stable current source with a noise level of only 20 μA on output current pulses of up to 4 A amplitude. We used the digital to analog converter to provide square pulses to the QCL driver. In comparison to the Stanford Research Systems DG-535 pulse generator used initially, the voltage pulses delivered by the D/A converter via the FPGA program were very stable over the entire 0-10 V range of the device. It was found that the pulses delivered by the DG-535 above ~ 4.5 V in amplitude were very noisy and caused the drive current of the QCL driver to fluctuate, as the amplitude of the drive current followed the input voltage pulses very precisely. A stand-alone program was written in Labview to run on the FPGA which allowed easy adjustment of the duration, repetition rate, and

amplitude of the voltage pulses. This was very convenient for determining the optimum parameters for driving the laser, allowing adjustable pulse duration up to continuous wave operation.

The piezo mirror mount in the Fabry-Perot was initially controlled by a Thorlabs MDT 693A, a piezo controller with 3 independent channels. The output voltage range of the controller is 0-150 V. Once it was determined that all 3 axes could be driven simultaneously, this controller was replaced by a single amplifier (VF-90-30150) plug in module for the cRIO. Fine adjustment of each individual axis was performed manually by turning thumbscrews on the mirror mount to make this mirror parallel to the fixed mirror. The amplifier module was controlled by a second program on the FPGA that allowed adjustable motion control through a Labview interface running on a PC. One of the advantages of using an FPGA is that separate programs can be loaded on different areas of the chip (different sets of logic gates) and run in parallel (true parallel processing). A control voltage originating from the D/A module was fed into the input of the amplifier. This control voltage was in the form of a modified sine wave. The voltage was changed (increased/decreased) linearly through most of the range from 0 to 3.75 V. The amplifier produces voltages between 0 and 150 V over the range of input voltages from 0 to 3.75 V. To accommodate the inertia of the mirror, the voltage was changed more slowly (in the form of a sine wave) near the turning points (0 and 3.75 V) where the mirror changed direction. The resulting waveform was a triangular wave with the sharp corners replaced by sine wave sections. The frequency of the waveform was adjustable in order to control the scanning speed of the piezo-driven mirror.

The FPGA program also controls data acquisition through two inputs of the NI 9223 Analog input module plugged into the cRIO chassis. Each input of this module is capable of simultaneously acquiring data at a maximum rate of 1MS/s. One channel monitors the output of the voltage waveform controlling the position of the piezo driven mirror, and a second channel samples the detector.

The FPGA program controls all of the above functions with highly precise timing and essentially no latency. For the purposes of testing various configurations of the laboratory model, another program runs on a personal computer to allow interactive adjustments to be made to the adjustable parameters outlined above (piezo control voltage, laser driver control pulses, sampling rates for the analog inputs). Likewise, the PC interface program allows the data from the analog inputs to be plotted. The position (piezo voltage) is plotted in the x-axis and the signal from the detector is plotted in the y-axis. So, the signal from the detector is plotted as a function of the position of the mirror and the spectrum is displayed on the computer monitor.

The final step for integration of the entire control system into a single box will be to replace the QCL driver with a plug in module for the cRIO.

CHAPTER 9: FANO REFLECTORS

9.1 Introduction

The Fabry-Perot interferometer in our ICLAS system requires very high reflectivity low loss mirrors. One of the common infrared materials in our working wavelength (3-12 μm) is ZnSe. Such a pair of wedged optics with high reflecting coating (>97.5%) on one side and anti-reflection coating on the other side cost ~ $1000. Thus, there is a good reason to explore other alternatives to fabricating high reflectivity FP optics, which might be suitable for low-cost mass production using methods of silicon device foundries.

We tested so-called Fano reflectors, obtained from University of Texas Arlington, where they were designed and fabricated by Prof. Weidong Zhou. These are two-dimensional photonic crystals (2D PC), due to strong interaction between in plane guided modes and vertical radiation modes, Fano resonances occur in these crystals with extremely high reflections [61]. A wide band of reflection can be obtained by controlling the design parameters. Two types of Fano reflectors, differ by the material type, were tested here.

9.2 Silicon On Insulator (SOI)

A schematic of silicon on insulator (SOI) reflector is shown in Fig 9.1. It was prepared from a silicon-on-oxide wafer that consisted of 3 μm SiO_2 on a Si substrate and then 2 μm Si on

top of the oxide. A pattern of circular holes was formed in the thin silicon with a period *a* of 5.7 μm. The reflectivity of such a design depends on the radius *r* of these holes and the refractive index surrounding it. The radii of the holes were 1.25 (sample #11) and 2 μm (sample #12).

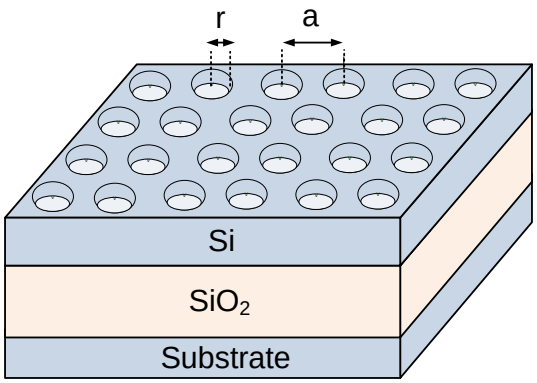

Figure 9.1 : Schematic of Fano reflector on silicon on insulator (SOI).

The transmission spectra of these two samples were compared with that of ZnSe mirrors used in the FP interferometer and are presented in Fig 9.2. While the ZnSe transmits 3%, and reflects 97%, in agreement with its design specifications, the Fano reflectors transmit zero (within experimental uncertainty) inside their designed HR band. The QCL wavelengths used in the external cavity configuration are indicated by arrow in Fig 9.2. Though both the wavelengths lie on the edge of the reflection band, with proper design it is possible to make this band lie exactly in our required wavelength regions. The fast and strong oscillations on either side of the band are resonances within the silicon substrate of the Fano reflector. Those oscillations have smallest amplitude on the low frequency side of the HR band, due to absorption by oxide, which lowers the *Q* of the optical cavity formed by the substrate. This absorption is demonstrated

separately in Fig. 9.2 (pink line) by the transmission spectrum of a silicon wafer on which a thick oxide was grown.

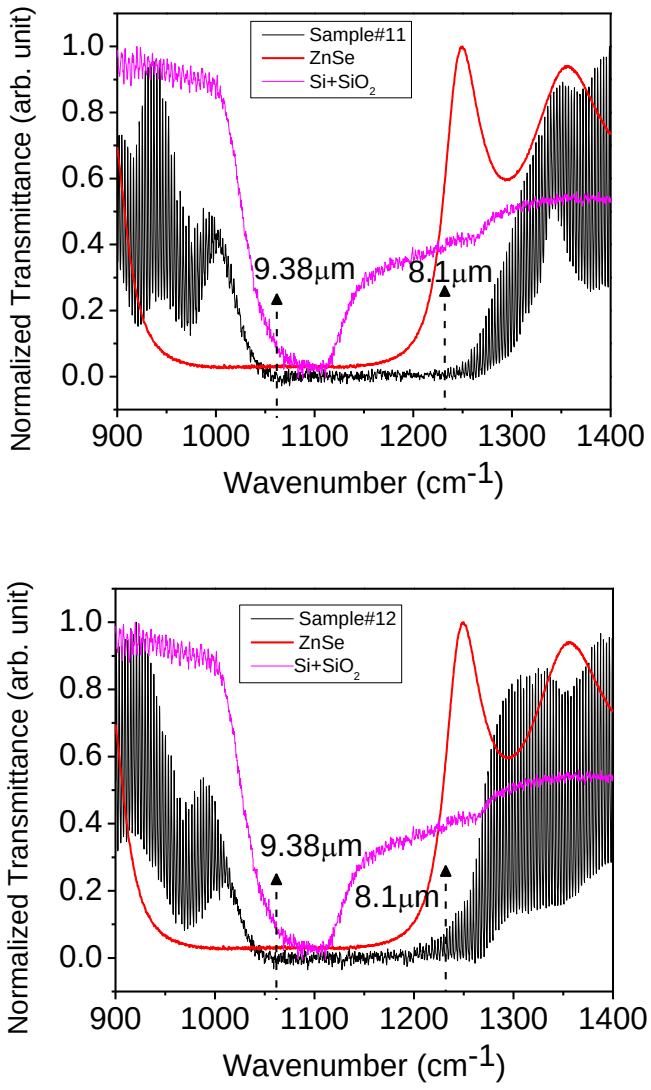

Figure 9.2 : Transmission spectra of Fano reflectors on SOI compared with the transmission of ZnSe mirror and SiO_2. The top figure is for sample # 11(r =1.25 μm) and the bottom is for sample # 12 (r =1.25 μm).

9.3 Suspended patterned membrane on Glass

The second type of Fano reflector we tested was suspended patterned Si membrane on glass substrate. The entire fabrication process of these samples can be found in [62]. This sample has a broad reflection band in 70-78 μm wavelength regions.

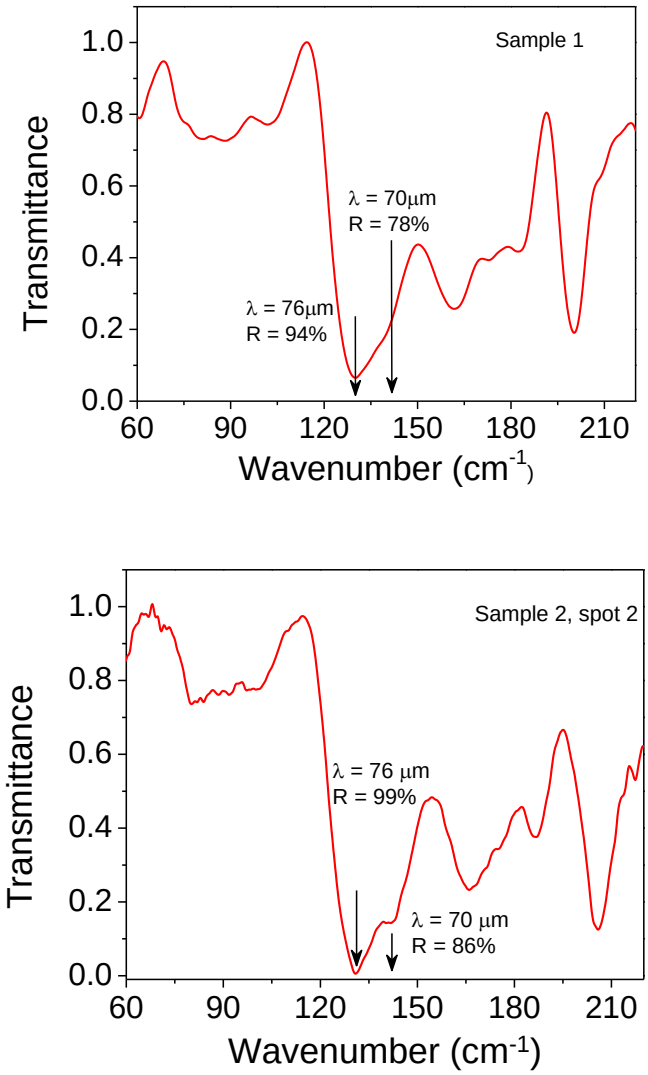

Figure 9.3 : Transmission spectrum of 70-76 μm band Fano Reflectors (top, sample 1), (bottom, sample 2) measured by FTIR.

By varying the holes diameter and the period of this structure, the mid-IR range can also be covered. We measured the transmission spectra of these samples by FTIR and the data are presented in Fig 9.3 for two different samples for different reflectivities. A globar source, 12 μm thick mylar beamsplitter and DTGS detector were used for this measurement. There is a clear high reflection band centered at 76 μm wavelength.

CHAPTER 10: IR ABSORPTION SPECTRA OF 2,4,6-TRINITROTOLUENE

10.1 Introduction

Knowledge of the infrared absorption spectra of low vapor pressure compounds in vapor phase is important for ICLAS system. The standard database has the vapor spectra (mid-IR region) of limited number of compounds. Thus, there is an opportunity to measure the vapor spectra of these compounds for the ICLAS application. This chapter presents the IR spectrum of 2,4,6-trinitrotoluene (TNT) measured using a high resolution BOMEM DA 8.01 FTIR spectrometer. The experimental results were compared with the literature.

10.2 Experiment

Figure 10.1 shows the schematic of the setup. A beam-folding plane mirror was mounted to intercept the collimated output beam from the external port of the spectrometer (BOMEM) and direct it to a 4 inch diameter off axis paraboloidal mirror at the proper angle. The latter mirror brought the beam to a focus at a distance of ~ 30 cm, such that an image of the spectrometer source aperture was formed at the focus. Both mirrors were mounted with push-pull screws that permitted complete alignment flexibility. The focused beam path was parallel to the incident collimated beam path, but shifted laterally by about 6 inches. After the focus the beam diverged

and was intercepted by a spectrometer detector module. The optical system was aligned initially using a quartz-halogen source and quartz beamsplitter from the spectrometer.

The vapor spectra of TNT were collected at different temperature using a KBr beamsplitter and a globar source. Nitrogen gas was blown for 10 minutes inside the gas tube to eliminate the water vapor and solid TNT powder was placed inside the tube with its two ends closed by 300 μm thick Si windows. A 77 K cooled HgCdTe detector was used to collect the spectrum and the spectrometer was operated at a resolution of 6 cm^{-1} to eliminate the Fabry-Perot oscillations arising from the Si windows. The tube was heated with heating tape wrapped around it and then shielded with copper sheet. Temperature was monitored with a sensor directly connected to the surface of the tube.

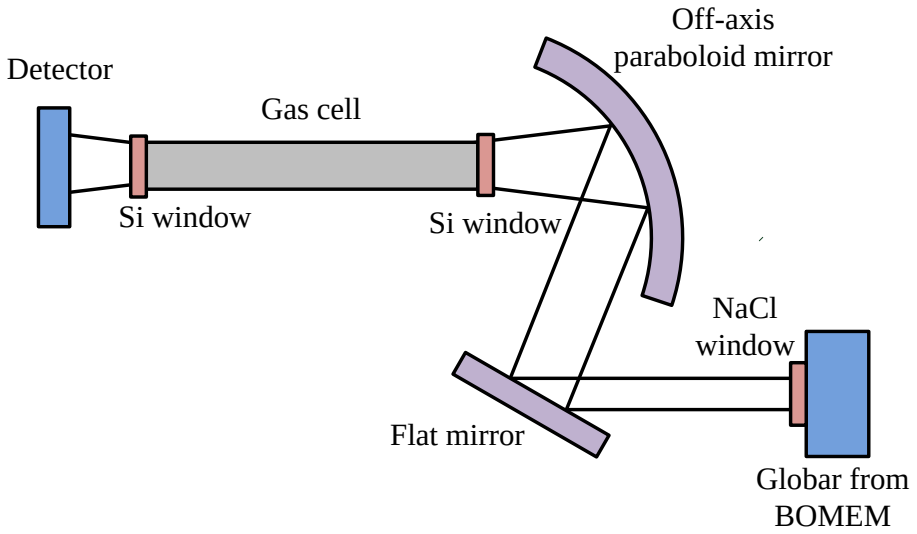

Figure 10.1 : Schematic of the experimental set up for measuring TNT in gas phase.

10.3 Results

The collected TNT spectrums at different temperature were presented in Fig 10.2. Significant vapor lines were observed in the 1000-3500 cm^{-1} spectral range when the temperature was raised above 140^{o}C.

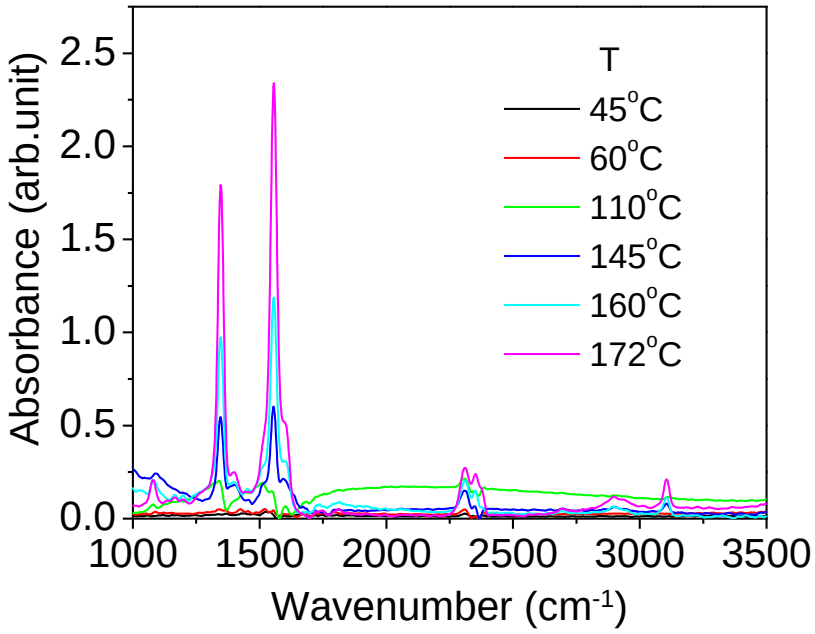

Figure 10.2 : Absorption spectra of TNT measured in a 10 cm gas cell and by FTIR spectrometer in 1000-3500 cm^{-1} range for different temperatures..

The measured data are compared with literature [63] and are presented in Table. 10.1.

Table 10-1: Infrared absorption lines of 2,4,6-trinitrotoluene

Experiment (cm^{-1})	Literature [63] (cm^{-1})
1076	1080
1345	1349
1407	1402
1554	1559
1607	1606
2907	2898
3100	3107

The spectrum is dominated by the symmetric and antisymmetric $-NO_2$ stretches at 1349 (7.41 μm) and 1559 (6.41 μm) cm^{-1} respectively [56]. A closer inspection of this stretching is shown in Fig 10.3 in the 5.5-8 μm wavelength range. The experimental curve matches nicely with the literature [63]. There is a clear evidence of broad absorption lines growing with rising temperature. The measured linewidths were ~ 30 cm^{-1}.

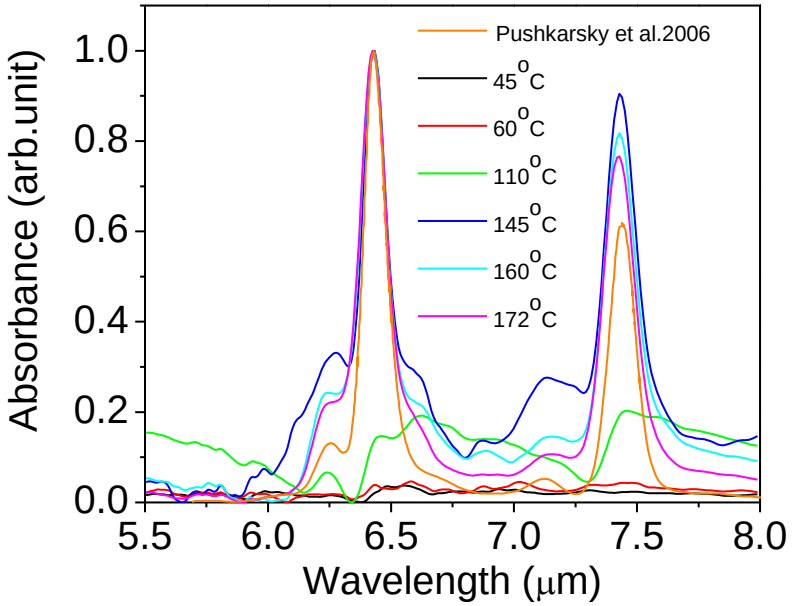

Figure 10.3 : Absorption spectra of TNT in 5.5-8 μm wavelength range for different temperatures compared with [64]. The spectrum is dominated by the symmetric and antisymmetric -NO_2 stretches at 7.41 μm 6.41 μm.

CHAPTER 11: CONCLUSIONS

We demonstrated a spectral sensing method with sufficient sensitivity to detect vapors of low vapor-pressure compounds, such as explosives. The method is Intracavity Laser Absorption Spectroscopy (ICLAS) at Long-Wave IR (LWIR, 8-12 μm wavelengths) using an external cavity quantum cascade laser and Fabry-Perot interferometer.

The sensitivity to vapors of a THz QCL ICLAS system at 69.9 μm was first estimated by the numerical solution of the laser rate equations to show the feasibility of kilometer effective active-cavity path lengths, and sensitivity to concentrations of 10 ppb, which is comparable to the concentrations of TNT at saturated vapor pressure. Implementation of the THz QCL-based ICLAS system proved difficult due to the requirement for a cryostat to house the laser and presence of strong water vapor lines in THz regime.

Next, a 9.38 μm QCL external cavity system was demonstrated. Fine mode structures from the external cavity operation were measured by FTIR spectrometer with a mode spacing of 0.05 cm^{-1}. A high resolution Fabry-Perot analyzer shows a resolution better than 0.5 cm^{-1}, which suffices for the expected pressure broadened vapor line widths of at least 0.2 cm^{-1}.

Next, an external cavity QCL at 8.1 μm wavelength with one facet AR coated and the other facet HR coated was demonstrated. A fine mode structure of mode spacing 0.03 cm^{-1}, was observed in this ICLAS system. The response of the laser emission spectrum for an open cavity QCL to the intracavity absorption of acetone vapor at 8.1 μm wavelength was demonstrated. The sensitivity limit for acetone based on the attenuation of the total power inside the cavity was

found to be ~0.1 Torr. The laser emission spectrum shifts by 6 cm^{-1} towards higher frequency in presence of acetone vapor at an estimated partial pressure of 165 mTorr corresponding to ~200 ppm. Assuming a minimum detectable shift of 0.03 cm^{-1}, which is the observed external cavity mode spacing, the sensitivity limit for acetone using the given set-up is estimated to be ~320 ppb. The sensitivity of this system was enhanced by six orders when it was combined with a fixed Fabry-Perot interferometer. The cavity is highly sensitive to the presence of water vapor in air with absorption coefficient 3×10^{-7} cm^{-1} or 111 ppm. The sensitivity limit to acetone, whose cross section is much higher, is thus 510 ppt.

The transmission spectra of Fano reflectors centered at 9 μm and 76 μm band, as a high reflectivity Fabry-Perot mirrors are also reported here. Two types of Fano reflectors (i) Silicon on Insulator (SOI) and (ii) suspended patterned membrane on glass are reported here. The measurement shows a reflectivity of ~ 99% which is promising for our system. This reflector can entirely substitute the expensive ZnSe mirrors for FP.

Finally the infrared absorption spectrum of 2,4,6-trinitrotoluene (TNT) at different temperature, measured by FTIR is presented. The spectra are dominated by symmetric and antisymmetric–NO_2 stretches at 7.41 μm and 6.41 μm wavelength.

APPENDIX A: LASER RATE EQUATION CODE

This program is written in FORTRAN to calculate the laser emission spectrum during time evolution when an absorption profile is inserted into the laser rate equation given by Eqs. 2.6 and 2.7.

```
      program ICLAS


      Integer q1,q2,q0

c     This part of the program contains all the input parameters.

      parameter(q1 = 73000)       c lower mode number
      parameter(q2 = 74600)       c upper mode number

      real*8 Rmq(q1:q2), RmqI(q1:q2), Bq(q1:q2), Rkq(q1:q2)
      real*8 A,B0,gamma,dt,P,Q,Rn,Rm,t,t1,t2,t0,t00,c,L

      q0 = 73800            c mode number at 8.1 micron
      Q = 4000              c HWHM of the gain in terms of mode number.
                            c This is corresponds to 120 cm-1 wavenumber.

      gamma = 3.9d10        c rate of broadband cavity loss
      B0 = 0.5              c peak gain at central wavelength
      A = 7.1d6             c.decay rate from upper level
      P = 1d19              c pump rate
      c = 3d10              c velocity of light
      dt = 1d-12            c iterations step in time
      t0 = 1d-9
      t00 = 1d-10
      t1 = 0                c initial time
      t2 = 1d-6             c final integration time
      L = 3d-1              c length of the external cavity
        wavelength = 8.D0

      pi = 3.14d0

c     This part of the program calculates the gain profile of the laser
c     and the intracavity absorber line profile


      open(33,file = 'absorption')
      Rn = 0d0                        c initial inversion = 0
      Do i = q1,q2
        Rmq(i) = 1d0                  c initial photon number = 1
        RmqI(i) = Rmq(i)
```

```
        Bq(i) = B0/(1.+((i-q0)/Q)**2)   c Lorentzian gain profile

c     second order polynomial fit of the acetone absorption cross section
c     to calculate the absorption coefficient profile varying the acetone
c     concentration


        Rkq(i) = 6.4d18*(7.92581d-20-2.10902d-24*i+1.40301d-29*i*i)


        write(33,*)real(i)/(6d-3*wavelength),Rkq(i)
      enddo
      close(33)

c     This part of the program saves the input data in a text file

      open(25, file = 'input.dat')
      write(25,*)' q0,Q,q1,q2:',q0,Q,q1,q2
      write(25,*)' gamma:',gamma
      write(25,*)' B0,A:',B0,A
      write(25,*)' P:',P
      write(25,*)' delta t =',dt,' end',t2
        write(25,*)' Absorption=1e-5, center=10002, halfwidth=5'
      write(25,*)' time, M, M_q/M, N :'
      close(25)

c     This part of the program does the iteration process to calculate the
c     photon number in individual laser mode and the laser inversion

      Do t = t1,t2,dt
        SumBM = 0d0
        Rm = 0d0
        Do i = q1,q2
          SumBM = SumBM+Bq(i)*Rmq(i)
          Rm = Rm+Rmq(i)
        enddo
        Do i = q1,q2
          Rmq(i) = Rmq(i)+dt*
     *       (-gamma*Rmq(i)+Bq(i)*Rn*(Rmq(i)+1)-Rkq(i)*c*Rmq(i))
          RmqI(i) = RmqI(i)+Rmq(i)
        enddo
          Rn = Rn+dt*(P-A*Rn-Rn*SumBM)

           if(mod(int(t/dt),int(t00/dt)).eq.0)then

        print*,real(t*1d9),'ns  M,Mq0/M,N:',
     ,  real(Rm),real(Rmq(q0)/Rm),real(Rn)

        open(25,file = 'output.dat',access = 'append')
        write(25,*)real(t*1e9),real(Rm),real(Rmq(q0)/Rm),real(Rn)
        close(25)
```

```
c     Saves the output in a text file

        open(24,file = 'output_full_3.dat',access='append')
                 Do i = q1,q2
                 write(24,*)int(t*1e9),i,i/60,
     ,           real(Rmq(i)),real(RmqI(i))
            enddo
           close(24)
        t00=t00*1.25

        endif

       enddo
       end
```

APENDIX B: PUBLICATIONS

Journal:

1. G. Medhi, P. Nandi, S. Mohan, G. Jose, 'Silver nanocluster formation in silicate glass by single step ion-exchange', Materials Letters, **61**, 2259-2261 (2007).
2. J. W. Cleary, G. Medhi, R. E. Peale, and W. R. Buchwald, 'Long-wave infrared surface plasmon grating coupler', Applied Optics, **49**, 16, 3102-3110, (2010).
3. G. Medhi, C. J. Fredricksen, R. E. Peale, A. V. Muravjov, H. Saxena, O. Edwards, 'Intracavity quantum cascade laser absorption sensor using Fabry-Perot Analyzer' (in preparation).
4. Monas Shahzad, Gautam Medhi, Robert E. Peale, Walter R. Buchwald, Justin W. Cleary, Richard Soref, Glenn D. Boreman, and Oliver Edwards, 'Infrared surface plasmons on heavily doped silicon', accepted Journal of Applied Physics, (2011).
5. J. W. Cleary, G. Medhi, M. Shahzad, R. E. Peale, G. D. Boreman, S. Wentzell, and W. R. Buchwald, 'Infrared surface polaritons on antimony', submitted Optics Express, (2011).

Conference Proceedings:

1. G. Medhi, A.V. Muravjov, H. Saxena, J.W. Cleary, C.J. Fredricksen, R.E. Peale, O. Edwards, "Infrared Intracavity Laser Absorption Spectrometer", Proc. SPIE 7680, 24 (2010).
2. G. Medhi, A. V. Muraviev, H. Saxena, J.W. Cleary, C. J. Fredricksen, R. E. Peale, and O. Edwards, "Infrared intracavity laser absorption spectrometer", in Proc. Intl. Symp. Spectral Sensing Research, (2010).
3. Gautam Medhi, Justin W. Cleary, Robert E. Peale, Glenn Boreman, Walter R. Buchwald, Sandy Wentzell, Oliver Edwards, and Isaiah Oladeji, "Infrared surface plasmon resonance hosts for sensors" in Photonics 2010: International Conference on Fiber Optics and Photonics, Indian Inst. Tech. Guwahati India, 11-15th Dec (2010).
4. Justin W. Cleary, Gautam Medhi, Robert E. Peale, Walter R. Buchwald, Oliver Edwards, and Isaiah Oladeji, "Infrared Surface Plasmon Resonance Biosensor", Proc. SPIE 7673, 5 (2010).
5. G. Medhi, A. V. Muravjov, H. Saxena, C. J. Fredricksen, T. Brusentsova, R. E. Peale, O. Edwards, "Intracavity laser absorption spectroscopy using mid-IR quantum cascade laser", Proc. SPIE 8032 - 12 (2011).
6. Monas Shahzad, Gautam Medhi, R. E. Peale, Ryuichi Tsuchikawa, Masahiro Ishigami, Walter Buchwald, Justin Cleary, Glenn D. Boreman, Oliver Edwards D. J. Diaz, and Ted A. Gorman, "Infrared surface waves on semiconductor and conducting polymer", Proc. SPIE 8024 - 2 V. 7 (2011).

7. Nima Nader Esfahani, Christopher J. Fredricksen, Guatam Medhi, R. E. Peale, Justin W. Cleary, Walter R. Buchwald, Himanshu Saxena , Oliver J. Edwards, "Plasmon resonance response to millimeter-waves of grating-gated InGaAs/InP HEMT" Proc. SPIE 8023 - 27 V. 1 (2011).
8. P. Figueiredo, J. Nath, G. Medhi, A. Muraviev, C. J. Fredricksen, W. R. Buchwald, J. W. Cleary, R. E. Peale, "Planar integrated plasmonic mid-IR spectrometer", Proc. SPIE 8155A - 2 (2011), Invited.
9. R. E. Peale, Nima Nader Esfahani, Christopher J. Fredricksen, Gautam Medhi, Justin W. Cleary, Walter R. Buchwald, Himanshu Saxena , Oliver J. Edwards, Ben D. Dawson, and M. Ishigami, "InP- and graphene-based grating-gated transistors for tunable THz and mm-wave detection", Proc. SPIE 8164 - 7 (2011).

REFERENCES

[1] E. A Sviridenkov. “Intracavity laser spectroscopy,” in *Proc. SPIE 3342,* 1998, pp. 1-21.

[2] W. Demtroder. *Laser Spectroscopy volume 2 Experimental Techniques*. Germany: Springer, 2008, pp. 1-75.

[3] J. U. White. “Long Optical Paths of Large Aperture.” *Journal of the Optical Society of America A, vol.* 32, pp. 1-4, 1942.

[4] J. Yinon. *Forensic and Environmental Detection of Explosives*. England: John Wiley & Sons Ltd., 1999.

[5] R. E. Peale, A. V. Muravjov, C. J. Fredricksen, G. D. Boreman, H. Saxena, G. Braunstein, V. L. Vaks, A. V. Maslovsky, S. D. Nikifirov. “Spectral signatures of acetone from ultraviolet to millimeter wavelengths,” in *Proc. 2006 Intl. Symp. Spectral Sensing Research,* 2006.

[6] L. Sinitsa. “Intracavity laser spectroscopy,” in *Proc. SPIE 4063*, 2000, pp. 26-38.

[7] R. Böhm, A. Stephani, V. M. Baev, and P. E. Toschek. “Intracavity absorption spectroscopy with a Nd^{3+}-doped fiber laser.” *Optics Letters*, vol. 18, pp. 1955-1957, Nov. 1993.

[8] A. Hugi, R. Maulini, and J. Faist. “External cavity quantum cascade laser.” *Semiconductor Science and Technology*, vol. 25, pp. 1-14, Aug. 2010.

[9] V. M. Baev, V. P. Dubov, and E. A. Sviridenkov. “Enhancement of the sensitivity of intracavity laser spectroscopy by the use of neodymium glass lasers.” *Soviet Journal of Quantum Electronics*, vol. 15, pp. 1648, 1985.

[10] T. P. Belikova, E. A. Sviridenkov, and A F. Suchkov. “Investigation of weak absorption and gain lines of some gases by the method of selective losses in a laser resonator.” *Soviet Journal of Quantum Electronics*, vol. 4, pp. 454-456, Apr. 1974.

[11] T. P. Belikova, E. A. Sviridenkov and A. F. Suchkov. “Highly Excited Vibrational-Rotational States of Molecules by the Method of Selective Losses in the Resonator of a Laser,” *Optics and Spectroscopy*, vol. 37, 1974.

[12] J. Sierks, T. Latz, V. M. Baev, and P. E. Toschek. “Enhancement of the sensitivity of a multimode dye laser to intracavity absorption.” *Optics Communications*, vol. 96, pp. 81–86, 1993.

[13] J. Sierks, T. Latz, V. Baev, and P. Toschek. “Dynamics of a cw multimode dye laser.” *Physical Review A*, vol. 57, pp. 2186-2203, Mar. 1998.

[14] D. A. Gilmore, P. V. Cvijin, and G. H. Atkinson. “Intracavity absorption spectroscopy with a titanium: sapphire laser.” *Optic Communications*, vol. 77, pp. 385-389, 1990.

[15] A. Kachanov, A. Charvat, and F. Stoeckel. “Intracavity laser spectroscopy with vibronic solid-state lasers. I. Spectro temporal transient behavior of a Ti:sapphire laser.” *Journal of the Optical Society of America B*, vol. 11, pp. 2412-21, Dec. 1994.

[16] L. F. Mollenauer, "Color center lasers." in *Laser Handbook*, Vol. 4. M. L. Stitch and M. Bass, North-Holland, Amsterdam: Elsevier Science Ltd. 1985, pp. 145–230.

[17] R. Beigang, G. Litfin, H. Welling. "Frequency behaviour and linewidth of cw single-mode color-center lasers." *Optics Communications*, vol. 22, pp. 269-271, 1977.

[18] V. M. Baev, H. Schroder, P. E. Toschek, *Optic Communications*, vol. 36, 1981.

[19] V. M. K. V.M. Baev, V.F. Gamalij, B.D. Lobanov, E.F. Martynovich, E.A. Sviri-denkov, A.F. Suchkov. *Soviet Journal of Quantum Electronics*, vol. 9, 1979.

[20] E. A. V.P. Bulatov, Y.V. Matyagin, N.A. Raspopov, A.N. Savchenko and Sviridenkov. *Soviet Journal Quantum Electronics*, vol. 9, 1989.

[21] P. Taylor, V. P. Kochanov, V. I. Serdyukov, and L. N. Sinitsa. "Use of LiF Colour- centre Laser in Intracavity Laser Spectroscopy." *Optica Acta*, vol. 32, pp. 1273-1280, 1985.

[22] A.D. Bykov, V.A. Kapitanov, O.V. Naumenko, T.M. Petrova, V.I. Serdyukov, L. N. Sinitsa. "The laser spectroscopy of highly excited vibrational states of $HD_{16}O$." *Journal of Molecular Spectroscopy*, vol. 153, pp. 197-207, 1992.

[23] V. L. Velichanskij, S. E. Vinogradov, E. A. Sviridenkov, G. G. Kharisov. "In-resonator laser spectroscopy with semiconductor lasers." *JETP Letters*, vol. 61, pp. 91-94, 1995.

[24] V. M. Baev, J. Eschner, E. Paeth, R. Schuler, P. E. Toschek. "Intra-cavity spectroscopy with diode lasers." *Applied Physics. B*, vol. 55, pp. 463-477, 1992.

[25] J. Eschner, “Dynamik und Absorptionsempfindlichkeit eines Vielmoden-Lasers.” Ph.D. thesis, Hamburg, 1993.

[26] J. Faist, F. Capasso, D. L. Sivco, C. Sirtori, A. L. Hutvhinson, and Y. C. Alfred. “Quantum Cascade Laser.” *Science*, vol. 264, pp. 553-556, 1994.

[27] L. E. Myers, R. C. Eckardt, M. M. Fejer, and R. L. Byer. “Quasi-phase-matched optical parametric oscillators in bulk periodically poled $LiNbO_3$.” *Journal of Optical Society of America B*, vol. 12, pp. 2102-2116, 1995.

[28] Giacomo Scalari, Christoph Walther, Milan Fischer, Romain Terazzi, Harvey Beere, David Ritchie and Jerome Faist. “THz and sub-THz quantum cascade lasers,” *Laser & Photonics Review*, vol. 3, pp. 45-66, Feb. 2009.

[29] B. S. Williams. “THz quantum cascade lasers.” *Nature Photonics*, vol. 1, pp. 517-525, 2007.

[30] Mikhail A. Belkin, Jonathan A. Fan, Sahand Hormoz, Federico Capasso, Suraj P. Khanna, Mohamed Lachab, A. Giles Davies and Edmund H. Linfield. “Terahertz quantum cascade lasers with copper metal-metal waveguides operating up to 178 K.,” *Optics express*, vol. 16, pp. 3242-8, Mar. 2008.

[31] Mattias Beck, Daniel Hofstetter, Thierry Aellen, Jérôme Faist, Ursula Oesterle, Marc Ilegems, Emilio Gini and Hans Melchior. “Continuous wave operation of a mid-infrared semiconductor laser at room temperature.” *Science*, vol. 295, pp. 301-5, Jan. 2002.

[32] Y. Bai, S. Slivken, S. R. Darvish, and M. Razeghi. “Room temperature continuous wave operation of quantum cascade lasers with 12.5% wall plug efficiency.” *Applied Physics Letters*, vol. 93, pp. 021103, 2008.

[33] Jerome Faist, Thierry Aellen, Tobias Gresch, Mattias Beck, Marcella Giovannini. “Progress in quantum cascade lasers,” in *Mid Infrared Coherent Sources and Applications*, Majid Ebrahim-Zadeh, Irina T. Sorokina, Ed. Netherlands: Springer, 2008, pp. 171-192.

[34] Sushil Kumar, Chun Wang I. Chan, Qing Hu, John L. Reno. “A 1.8-THz quantum cascade laser operating significantly above the temperature of $\hbar\omega/k_B$.” *Nature Physics*, Vol. 7, pp. 166-171, 2011.

[35] J Q Liu, J Y Chen, L Li, F Q Liu, L J Wang, Z G Wang. “Terahertz quantum cascade lasers operating above liquid nitrogen temperature.” in *3rd International Photonics & OptoElectronics Meetings*, 2010, pp. 1-5.

[36] I Vurgaftman, C L Canedy, C S Kim, M Kim, W W Bewley, J R Lindle, J Abell and J R Meyer. “Mid-infrared interband cascade lasers operating at ambient temperatures.” *New Journal of Physics*, vol. 11, pp. 1-13, 2009.

[37] C. Gmachl, D. L. Sivco, R. Colombelli, F. Capasso, and A. Y. Cho. “Ultra-broadband semiconductor laser.” *Nature*, vol. 415, pp. 883-7, Feb. 2002.

[38] C. Luo, S. G. Johnson, and J. D. Joannopoulos. “All-angle negative refraction in a three-dimensionally periodic photonic crystal.” *Applied Physics Letters*, vol. 81, pp. 2352, 2002.

[39] J Faist, Claire Gmachl, Federico Capasso, Carlo Sirtori, Deborah L Sivco, James N Baillargeon, Alfred Y Cho. “Distributed feedback quantum cascade lasers.” *Applied Physics Letters*, vol. 70, pp. 2670-2672, 1997.

[40] C. Gmachl, Jerome Faist, James N. Baillargeon, Federico Capasso, Carlo Sirtori, Deborah L. Sivco, S. N. George Chu, and Alfred Y. Cho. “Complex-Coupled Quantum Cascade Distributed-Feedback Laser.” *IEEE Photonics Technology Letters*, vol. 9, pp. 1090-1092, 1997.

[41] K. Namjou, S. Cai, and E. A. Whittaker, J. Faist, C. Gmachl, F. Capasso, D. L. Sivco, and A. Y. Cho. “Sensitive absorption spectroscopy with a room-temperature distributed-feedback quantum-cascade laser.” *Optics letters*, vol. 23, pp. 219-21, Feb. 1998.

[42] S. W. Sharpe, J. F. Kelly, and J. S. Hartman, C. Gmachl, F. Capasso, D. L. Sivco, J. N. Baillargeon, and A. Y. Cho. “High-resolution (Doppler-limited) spectroscopy using quantum-cascade distributed-feedback lasers.” *Optics letters*, vol. 23, pp. 1396-8, Sep. 1998.

[43] A. A. Kosterev and F. K. Tittel. “Chemical Sensors Based on Quantum Cascade Lasers.” *IEEE Journal of Quantum Electronics*, vol. 38, pp. 582-591, 2002.

[44] Benjamin G. Lee, Mikhail A. Belkin, Ross Audet, Jim MacArthur, Laurent Diehl, Christian Pflügl, Federico Capasso, Douglas C. Oakley, David Chapman, Antonio Napoleone, David Bour, Scott Corzine, Gloria Höfler, Jérôme Faist. “Widely tunable

single-mode quantum cascade laser source for mid-infrared spectroscopy." *Applied Physics Letters*, vol. 91, pp. 231101, 2007.

[45] Benjamin G. Lee, Haifei A. Zhang, Christian Pflügl, Laurent Diehl, Mikhail A. Belkin, Milan Fischer, Andreas Wittmann, Jerome Faist, and Federico Capasso. "Broadband Distributed-Feedback Quantum Cascade Laser Array Operating From 8.0 to 9.8 μm," *IEEE Photonics Technology Letters*, vol. 21, pp. 914-916, Jul. 2009.

[46] G. P. Luo, C. Peng, H. Q. Le, S. S. Pei, W.-Y. Hwang, B. Ishaug, J. Um, James N. Baillargeon, and C.-H. Lin. "Grating-tuned external-cavity quantum-cascade semiconductor lasers," *Applied Physics Letters*, vol. 78, pp. 2834, 2001.

[47] G. Totsching, F. Winter, V. Pustogov, J. Faist and A. Muller. "Mid-infrared external-cavity quantum cascade laser." *Optics letters*, vol. 27, pp. 1788-90, 2002.

[48] G. P. Luo, C. Peng, H. Q. Lee, S. S. Pei, H. Lee, W. Y. Hwang, B. Ishaug and J. Zheng. "Braodly wavelength-tunable external cavity mid-infrared quantum cascade lasers." *IEEE Journal of Quantum electron*, vol. 38, pp. 486-94, 2002.

[49] J. Faist, M. Beck, T. Aellen, and E. Gini. "Quantum-cascade lasers based on a bound-to-continuum transition." *Applied Physics Letters*, vol. 78, pp. 147, 2001.

[50] R. Maulini, M. Beck, J. Faist, and E. Gini. "Broadband tuning of external cavity bound-to-continuum quantum-cascade lasers." *Applied Physics Letters*, vol. 84, pp. 1659, 2004.

[51] T. Tsai and G. Wysocki. “Fast Wavelength Tuning of External Cavity Quantum Cascade Lasers.” *in Lasers and Electro-Optics, 2009 and 2009 Conference on Quantum electronics and Laser Science Conference. CLEO/QELS 2009*, pp. 1-2, 2009.

[52] H. Q. Le and B. Ishaug. “Broadly wavelength-tunable external cavity, mid-infrared quantum cascade lasers.” *IEEE Journal of Quantum Electronics*, vol. 38, pp. 486-494, May. 2002.

[53] V. M. Baev, T. Latz, and P. E. Toschek. “Laser intracavity absorption spectroscopy.” *Applied Physics B*, vol. 69, pp. 171-202, 1999.

[54] S. Kumar, Q. Hu, and J. L. Reno. “186 K operation of terahertz quantum-cascade lasers based on a diagonal design.” *Applied Physics Letters*, vol. 94, p. 131105, 2009.

[55] S. Kumar, B. S. Williams, S. Kohen, Q. Hu, and J. L. Reno. “Continuous-wave operation of terahertz quantum-cascade lasers above liquid-nitrogen temperature.” *Applied Physics Letters*, vol. 84, pp. 2494, 2004.

[56] C.J. Wysocki, P. Dalton, M.J.Brody, H.J. Lawley. “Acetone odor and irritation thresholds obtained from acetone-exposed factory workers and from control (occupationally unexposed) subjects.” *American Industrial Hygiene Association Journal*, vol. 58, pp. 704-12, 1997.

[57] Q. K. Yang, B. Hinkov, F. Fuchs, W. Bronner, K. Köhler, J. Wagner, R. Maulini and J. Faist. “Rate equations analysis of external-cavity quantum cascade lasers.” *Journal of Applied Physics*, vol. 107, pp. 043109, 2010.

[58] H. A. Gebbie. “Atmospheric Transmission in the 1 to 14 micron region.” *Proc. Roy. Soc A.*, vol. 206, 1951.

[59] R. D. Hudson. *Infrared System Engineering*. New York: John Wiley & Sons, 1969.

[60] J. G. Cormier and J.T.Hodges. “Infrared water vapor continuum absorption at atmospheric temperatures.” *The journal of chemical physics*, vol. 122, pp. 114309, 2005.

[61] Z. Qiang, H. Yang, S. Member, S. Chuwongin, and D. Zhao. “Design of Fano Broadband Reflectors on SOI.” *IEEE Photonics Technology Letters*, vol. 22, pp. 1108-1110, 2010.

[62] H. Yang, Z. Qiang, L. Chen, H. Pang, Z. Ma, and W. Zhou. “Surface-Normal Fano Filters and Broadband Reflectors Based on Transferred Silicon Nanomembranes on Glass Substrates.” in *2008 8th IEEE Conference on Nanotechnology*, vol. 2, 2008, pp. 209-210.

[63] J. Janni, B. D. Gilbert, R. W. Field, and J. I. Steinfeld. “Infrared absorption of explosive molecule vapors.” *Spectrochimica Acta Part A: Molecular and Biomolecular Spectroscopy*, vol. 53, pp. 1375-1381, Aug. 1997.

[64] M. B. Pushkarsky, I. G. Dunayevskiy, M. Prasanna, A. G. Tsekoun, R. Go, and C. K. N. Patel. “High-sensitivity detection of TNT.” in *Proceedings of the National Academy of Sciences of the United States of America*, vol. 103, 2006, pp. 19630-4.